Investigating the therapeutic potential of AMP-activated protein kinase in Myotonic Dystrophy Type 1

By Naomi Misquitta

A thesis submitted to the University of Ottawa in partial fulfillment of the requirements for the Master of Science degree in Cellular and Molecular Medicine

Department of Cellular & Molecular Medicine
Faculty of Medicine
University of Ottawa

Abstract

Myotonic dystrophy type 1 (DM1) is the most prevalent form of adult-onset muscular dystrophy and arises from a CTG trinucleotide repeat expansion mutation in the dystrophia myotonica protein kinase (*DMPK*) gene. Mutant DMPK mRNAs accumulate as nuclear foci and cause disruptions in pre-mRNA processing via a toxic gain-of-function mechanism that involves the misregulation of key RNA-binding proteins, such as muscleblind-like splicing regulator 1 (MBNL1). These misregulations result in perturbations in pre-mRNA alternative splicing, amongst other cellular processes, which promote skeletal muscle impairments and give rise to several clinical features of DM1 including weakness, wasting, and myotonia. To date, there is no cure for DM1.

AMP-activated protein kinase (AMPK) signaling is a key regulator of skeletal muscle plasticity that was initially revealed by the Jasmin Laboratory to be impaired in a mouse model of DM1. Our lab also demonstrated that potent AMPK activators, AICAR and exercise, improve the disease phenotype in DM1 mouse skeletal muscles. Here, we examined the combinatorial impact of these AMPK agonists on the DM1 skeletal muscle phenotype. Our findings revealed that, in combination, 4 weeks of swimming exercise and AICAR treatment additively mitigate the nuclear accumulation of toxic RNA foci and promote muscle fiber hypertrophy in the skeletal muscles of female DM1 mice. These combinatorial effects were accompanied by a concomitant reduction in both the misregulation of MBNL1 and aberrant alternative splicing of key pre-mRNA targets. Altogether, these results highlight the therapeutic potential of combining AMPK-based interventions for the treatment of DM1.

Acknowledgements

I would like to thank my supervisor, Dr. Bernard Jasmin, for the opportunity to pursue graduate studies in the Jasmin Laboratory and for his support over the past few years.

As well, I would like to express my gratitude to the members of my thesis advisory committee, Dr. Mary-Ellen Harper, Dr. Lynn Megeney and Dr. Morgan Fullerton, for their guidance and expertise throughout this project.

A special thank you to Dr. Christine Péladeau, Dr. Guy Bélanger, and Kristen Marcellus for their help in training me on various techniques (especially the RNA extraction!), and to Dr. Aymeric Ravel-Chapuis for his guidance throughout this work.

To Amanda Tran and John Lunde, thank you for your technical assistance with all the ACVS procedures, completing this study would not have been possible without your dedicated support.

I would also like to express my gratitude to Dr. Kerstin Ure and Sarah from the Behaviour & Physiology Core and Dr. Chloë van Oostende-Triplet and Redaet from the Cell Biology & Image Acquisition Core for their technical expertise with the swimming exercise protocol and microscopy workflows, respectively.

To the past and present members of the Jasmin Laboratory, my fellow grad school buddies, and the RGN 3rd floor administrative and support staff, thank you for your friendship and collegiality.

A special thank you to my friends for cheering for me in Ottawa and from across the country.

Finally, to my wonderful family, I am deeply grateful for your unwavering love, support, encouragement, and prayers.

Funding

This study was supported by grants from the Association Française Contre les Myopathies, Muscular Dystrophy Association and Muscular Dystrophy Canada. N.M. was supported by a Canadian Institute for Health Research Canada Graduate Scholarship, Queen Elizabeth II Scholarship in Science & Technology, and Dr. Éric Poulin Centre for Neuromuscular Disease STaR Award throughout this work.

Preface

The following sections of this thesis were previously published (1) in *Human Molecular Genetics* in January 2023 with some amendments made thereafter: Chapter 2: Materials & Methods, Chapter 3: Results, Figures (with respective captions): 3, 4, 5, 6, 7, 8, 9, 10, 11 and A1, and segments of Chapter 4: General Discussion.

Article Title: Combinatorial treatment with exercise and AICAR potentiates the rescue of myotonic dystrophy type 1 mouse muscles in a sex-specific manner

Author List: Naomi S. Misquitta, Aymeric Ravel-Chapuis, Bernard J. Jasmin

Publisher: Oxford University Press

Full Citation: Misquitta, N. S., Ravel-Chapuis, A., & Jasmin, B. J. (2023). Combinatorial treatment with exercise and AICAR potentiates the rescue of myotonic dystrophy type 1 mouse muscles in a sex-specific manner. *Hum. Mol. Genet.* 32(4), 551–566. https://doi.org/10.1093/hmg/ddac222

Table of Contents

List of Figures

List of Tables

List of Abbreviations

ACC	Acetyl-coA carboxylase
ACTA1	Skeletal muscle α-actin 1
AICAR	5-aminomidazole-4-carboxamide-1-β-D-ribofuranoside
AMPK	AMP-activated protein kinase
ASE	Alternative splicing event
ATP2A1	Sarco/endoplasmic reticulum Ca^{2+} transporting ATPase 1
BIN1	Bridging-integrator 1
CELF1	CUGBP Elav-like family member 1
CLCN1	Muscle-specific chloride channel 1
CUG^{exp}	CUG expansion
CII-SDHB	Mitochondrial succinate dehydrogenase iron-sulfur subunit (complex II)
CIV-MTCO1	Mitochondrially encoded cytochrome c oxidase I (complex IV)
CV-ATP5A	Mitochondrial ATP synthase F1 subunit alpha (complex V)
DAPI	4′,6-diamidino-2-phenylindole
DMD	Duchenne muscular dystrophy
DMPK	Myotonic dystrophy protein kinase
DM1	Myotonic dystrophy type 1
EDL	Extensor digitorum longus
FISH	Fluorescent *in situ* hybridization
GAPDH	Glyceraldehyde 3-phosphate dehydrogenase
GSK3β	Glycogen synthase kinase 3β
HSA^{LR}	Human skeletal actin long-repeat
HSA^{SR}	Human skeletal actin short repeat
MBNL1	Muscleblind-like splicing regulator 1
mTORC1	Mammalian target of rapamycin complex 1
MHC	Myosin heavy chain
OXPHOS	Oxidative phosphorylation
PGC1α	Peroxisome proliferator-activated receptor gamma coactivator-1 alpha
RYR1	Ryanodine receptor 1
SDH	Succinate dehydrogenase
TA	Tibialis anterior
WT	Wild type
3’ UTR	3’ untranslated region

Chapter 1: General Introduction

1.1 Muscular Dystrophy

Muscular dystrophy refers to a group of inherited disorders that adversely impact skeletal muscle, the largest organ in the human body, to various extents and with diverse consequences. These conditions are caused by mutations in genes that are generally associated with the structure and function of skeletal muscle but may also influence these aspects in other tissues (2). The main symptoms of muscular dystrophy include muscle weakness and movement-related impairments that can progress over time and, in some cases, preferentially affect specific types of skeletal muscles (2). Given the essential roles of skeletal muscle in producing locomotion, regulating breathing, maintaining posture, and stabilizing joints, muscular dystrophy can significantly impact the performance of activities of daily living and contribute to reduced life expectancy in patients (3). To date, there remains a persistent need for the development of novel therapeutic interventions and, ideally, curative treatments for these conditions. In this thesis, I present a combinatorial therapeutic strategy targeting AMPK activation for a form of muscular dystrophy known as Myotonic Dystrophy Type 1.

1.2 Myotonic Dystrophy Type 1

Myotonic dystrophy type 1 (DM1) is an autosomal dominant neuromuscular disease with an estimated genetic prevalence of 1 in 2,100 births in a cosmopolitan population (4), and an estimated worldwide prevalence of 9.27 per 100,000 cases (5). The highest point prevalence of DM1, 158 in 100,000 (1 in ~600) individuals (6), has been reported in the geographical region of Saguenay-Lac-St. Jean, Quebec, Canada, due to a founder effect (7). As the most common form of muscular dystrophy diagnosed in adulthood, DM1 is characterized by myotonia (delayed relaxation following a voluntary muscle contraction) and progressive skeletal muscle weakness

and wasting (8), the latter of which has been attributed to the increased risk of premature death in DM1 patients (9,10). In addition to skeletal muscle abnormalities that typically impact the distal limb muscles and diaphragm, the symptoms of DM1 are multisystemic and can include cataracts, cardiac arrythmia, insulin resistance, gastrointestinal dysfunction, and cognitive decline (11,12). In separate cohorts of adult-onset DM1 patients, respiratory failure and adverse cardiac events were determined to be the major causes of DM1-associated mortality, with a median survival age of 59-60 years (9,10,13). To date, there is no cure for DM1 and current treatment recommendations, which include various interventions such as periodic cardiac evaluations, ventilation support, anti-myotonia medication and physical therapy, are limited to alleviating individual symptoms (14).

While DM1 is a complex, multisystemic disorder, a vast number of studies have focused on characterizing and mitigating the DM1 skeletal muscle phenotype given that impairments in this tissue [1] are the most common disease symptoms reported by patients (15), [2] serve as key predictors of DM1-associated mortality (3,9), and [3] can be more readily studied at the functional, cellular, and molecular levels in patients and well-established preclinical models. In this context, the scope of my thesis is limited to the study of DM1 in skeletal muscle; however, it is important to acknowledge that additional complexities in the pathophysiology and treatment of DM1 arise from its multisystemic and highly variable nature.

1.2.1 Pathomechanism of DM1: RNA Toxicity Paradigm

DM1 is caused by a cytosine-thymine-guanine (CTG) trinucleotide repeat expansion mutation in the 3’ untranslated region (UTR) of the dystrophia myotonica protein kinase (*DMPK*) gene (16,17). In the general population, healthy individuals typically carry 5-34 CTG repeats, whereas individuals with 35-49 repeats can remain asymptomatic but have an increased probability

of transmitting a larger CTG expansion to subsequent generations, resulting in a phenomenon known as genetic anticipation (18,19). In DM1, symptoms begin to manifest in individuals with expansion sizes that can range from 50 to >1000 repeats (18) from which five clinical subtypes based on the age of onset have been established: congenital (most severe), childhood/infantile, juvenile, adult, and late adult (most mild) (12,20). The length of the CTG expansion mutation has generally been shown to inversely correlate with the age at which symptoms arise in DM1 patients (20) (**Table 1**). However, the severity of disease is highly variable both between and within clinical subtypes with overlapping CTG size distributions (8,12). Findings from a correlational study in DM1 patients have indicated that respiratory function and skeletal muscle power strongly correlate with CTG repeat length after accounting for several confounding factors including sex and age (21), thereby emphasizing the complex relationship between DM1 genetics and resulting phenotypes.

Table 1. Clinical subtypes of DM1 based on the age of onset.

Phenotype	**CTG Length****	**Age of Onset***
Asymptomatic/Pre-Mutation	35-49	-
Late Adult	50-150	> 40 years
Adult/"Classical"	50-1000	20 to 40 years
Juvenile†	>800	10 to 20 years
Childhood/Infantile	>800	1 month to 10 years
Congenital	>1000	Birth to < 1 month

* Based on de Antonio *et al*. (12)

** Based on Seifert *et al.*(18) and the Muscular Dystrophy Association (22)

† Due to the lack of consensus on early-onset subtype distinctions (12), juvenile DM1 can also be categorized under the childhood form

Since the identification of its genetic basis (16,17), the etiology of DM1 has been shown to be influenced by multiple pathomechanisms. It was initially postulated that the DM1 phenotype arose from the haploinsufficiency of DMPK (23), a protein kinase that is highly expressed in cardiac and skeletal muscle and whose precise function(s) remain relatively unknown (24). Early studies demonstrated that *Dmpk* deficient mice display a mild to progressive myopathy and reduced force generation capacity (25,26), whereas more recent findings did not reveal significant skeletal muscle dysfunction in response to heterozygous or homozygous *Dmpk* deletion (24). Similarly, knockout experiments targeting *SIX5*, a neighboring gene with reduced expression levels in DM1 that lies adjacent to the CTG repeat expansion, revealed that *Six5* deficient mice develop cataracts (a symptom of DM1) without skeletal muscle abnormalities (27). Although *Dmpk* and *Six5* knockout studies characterize DM1 as a multigenic disorder, the lack of significant muscular involvement in these models revealed that both DMPK and SIX5 depletion are not sufficient to elicit the major clinical symptoms of DM1 in skeletal muscle (24,27).

The preferred model and major pathologic effect of the CTG repeat expansion occurs following transcription of the mutant *DMPK* allele and can be referred to as the RNA toxicity model of DM1 (**Figure 1**). CUG repeat expansions (CUG^{exp}) in mutant *DMPK* mRNA transcripts form hairpin-like structures that aggregate in the nucleus as distinct RNA foci (28,29). Through a toxic gain-of-function mechanism, CUG^{exp} RNA foci bind and sequester muscleblind-like splicing regulator 1 (MBNL1) (30–32), an RNA-binding protein that mediates the developmental transition from fetal to adult splice isoforms for MBNL1-targeted pre-mRNA transcripts (33–35). In addition to MBNL1 sequestration, the presence of CUG^{exp} foci has been shown to increase the activation and stabilization of CUG binding protein Elav-like family member 1 (CELF1) (36), another RNA-binding protein that antagonizes the role of MBNL1 in splicing regulation (37). Moreover, the

post-natal expression of CELF1 is abnormally elevated in DM1 which further exacerbates the missplicing of CELF1-regulated pre-mRNA transcripts (36,38–40). In addition to these two splicing regulators, several other RNA-binding proteins are known to also be misregulated in DM1 muscle including Staufen1, heterogenous nuclear ribonucleoprotein (hnRNP) A1, and hnRNP H (41–43).

The misregulation of RNA-binding proteins and, in particular, the sequestration of MBNL1 and upregulation of CELF1 cause disruptions in alternative splicing processes, generally resulting in the promotion of fetal mRNA splice isoforms whose protein counterparts can compromise downstream cellular functions (34,37,44). Therefore, DM1 is referred to as a spliceopathy (described in section 1.2.2). The disease-specific roles of these splicing factors have been extensively studied using overexpression and knockout models that recapitulate clinical features of DM1 skeletal muscle, thereby establishing MBNL1 and CELF1 as major RNA-binding proteins affected by CUG^{exp} RNA toxicity (33–35,39,45–48). Indeed, the majority of DM1-related splicing abnormalities and transcriptomic changes caused by CUG^{exp} RNA foci expression have been ascribed to the functional loss of MBNL1 (34,35,47,49). In contrast, CELF1 upregulation in mice gives rise to the dystrophic phenotype observed in DM1 skeletal muscle and further promotes a subset of DM1-related alternative splicing events (40,45). Similar experiments have also implicated Staufen1 and hnRNP A1 in the DM1 skeletal muscle spliceopathy, amongst other disease features such as muscle atrophy (41,50).

CUG^{exp} RNA toxicity was characterized as a primary pathomechanism of DM1 following the generation of the human skeletal actin long repeat (HSA^{LR}) mouse, a disease model that expresses approximately 250 CTG repeats in the 3' UTR of the human skeletal actin (*ACTA1*) transgene (51). The skeletal muscles of HSA^{LR} mice recapitulate the following characteristics of

DM1: nuclear RNA foci accumulation, MBNL1 sequestration, aberrant alternative splicing, myopathy, and myotonia, although CELF1 upregulation and skeletal muscle weakness and wasting are not robustly observed (34,51). In contrast, the expression of five CTG repeats in transgenic mice (classified as human skeletal actin short repeat or HSA^{SR}) did not reproduce the DM1 skeletal muscle pathology. The characterization of the tissue-specific HSA^{LR} and HSA^{SR} models provided proof-of-concept evidence that the presence of CUG^{exp} RNA induces toxic effects in skeletal muscle and is sufficient to produce hallmark features of the DM1 phenotype (51). In combination with similar observations in other transgenic DM1 mouse models (40,52,53), these findings have implicated RNA-mediated toxicity as a dominant mechanism of disease in DM1 skeletal muscle (54).

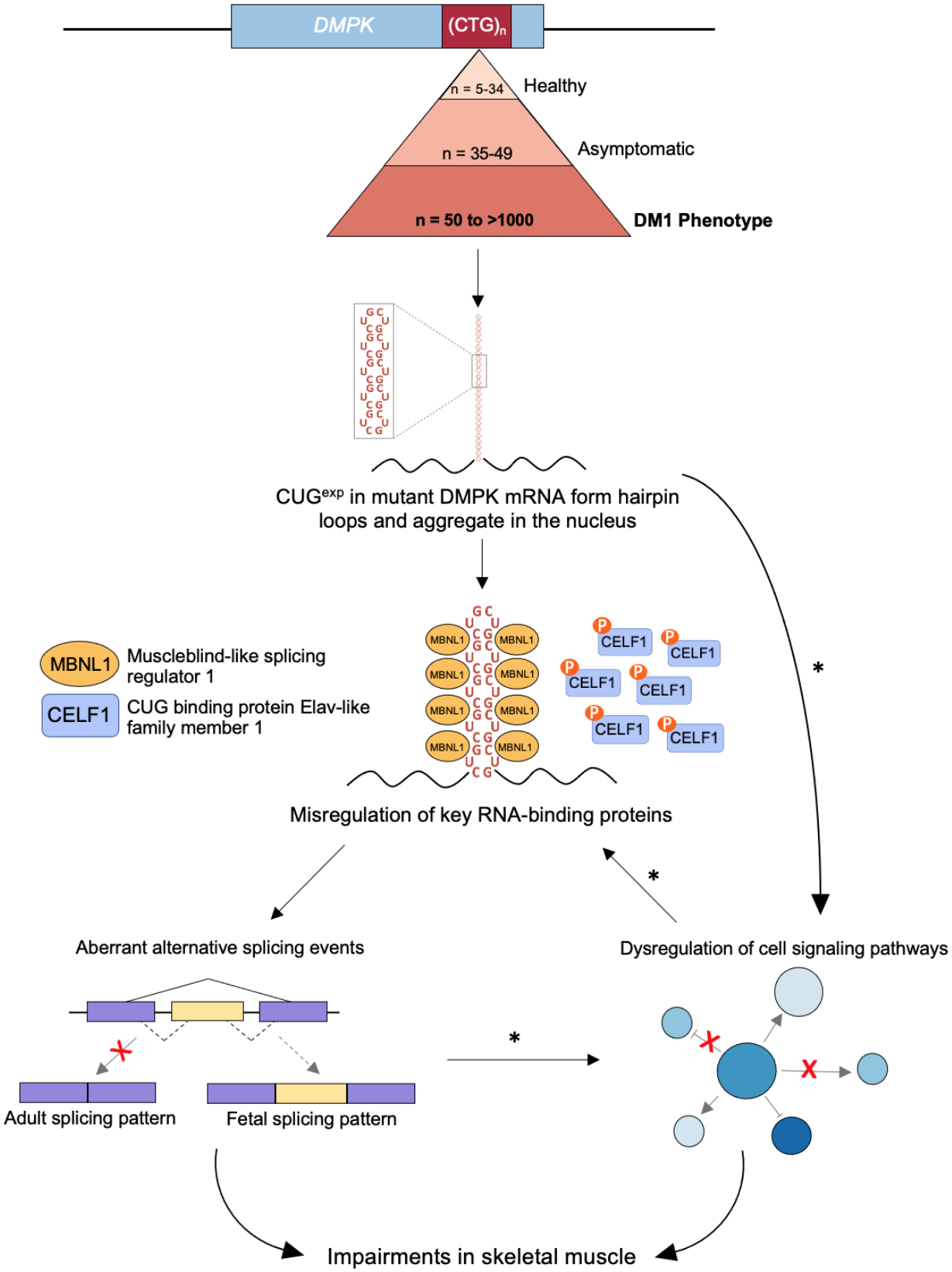

Adapted from Turner & Hilton-Jones (11) and Chau & Kalsotra (55).

Figure 1. The RNA toxicity paradigm of DM1. DM1 is caused by a CTG repeat expansion mutation in the *DMPK* gene. The size of the CTG expansion (n) that corresponds with the emergence of the DM1 phenotype ranges between 50 to >1000 repeats. Following transcription, CUG^{exp} in mutant DMPK mRNA transcripts form hairpin-like loops and accumulate in the nucleus as distinct foci. The toxic effect of CUG^{exp} RNA foci involves the misregulation of key RNA-binding proteins such as MBNL1 and CELF1. MBNL1 is sequestered by CUG^{exp} RNA foci, while the activity of CELF1 is upregulated in DM1. The functional depletion of MBNL1 and hyperactivation of CELF1, amongst other RNA-binding protein perturbations, results in the abnormal regulation of alternative splicing processes which favors the expression of fetal mRNA splicing patterns in adult tissues. The dysregulation of cell signaling pathways has also been suggested to arise from the presence of toxic CUG^{exp} RNA foci or aberrant alternative splicing events and further contribute to the disease pathology in skeletal muscle. The asterisk (∗) indicates that there is a limited amount of evidence for the underlying molecular mechanism(s) which, in general, remain uncharacterized.

1.2.2 DM1 Skeletal Muscle Spliceopathy

Aberrant alternative splicing is a cardinal molecular characteristic of DM1 that arises from CUG^{exp} RNA toxicity and the concomitant misregulation of RNA-binding proteins such as MBNL1. In healthy tissue, alternative splicing processes mediate the essential transition from fetal to adult mRNA splice isoforms for developmentally regulated genes. Splicing perturbations in DM1 generally involve the abnormal retention of fetal mRNA splicing patterns (34), which results in the production of fetal protein isoforms that cannot adequately support physiological functions in adult tissue. Multiple transcriptomic analyses of the DM1 splicing phenotype have collectively revealed an array of aberrant alternative splicing events (ASEs), several of which have been associated with disease symptoms in skeletal muscle (56–58).

A well-established DM1 ASE that underlies myotonia, the hallmark clinical feature of DM1, is the missplicing of voltage-gated chloride channel 1 (CLCN1) pre-mRNA transcripts (56,59,60). CLCN1 is preferentially expressed in adult skeletal muscle and has an integral role in regulating the electrical excitability of the sarcolemma (muscle fiber plasma membrane) (61). The influx of chloride ions via CLCN1 is necessary to restore and stabilize the resting membrane potential of the sarcolemma following its depolarization during excitation-contraction (EC) coupling (61). In healthy skeletal muscle, the post-natal splicing pattern of *CLCN1/Clcn1* pre-mRNA transcripts requires the MBNL1-mediated removal of fetal exon 7A to produce the functional protein in adult tissue (59,60). In DM1, the nuclear depletion of MBNL1 by CUG^{exp} RNA foci results in the aberrant inclusion of exon 7A which creates a premature stop codon in mature *CLCN1/Clcn1* mRNA (59,60). While *CLCN1/Clcn1* pre-mRNA alternative splicing is developmentally regulated by MBNL1 (35), CELF1 upregulation has been suggested to destabilize *CLCN1/Clcn1* mRNA transcripts independently of splicing processes (37). As a result,

CLCN1/Clcn1 mRNA isoforms that retain exon 7A are either degraded in the nucleus or exported to produce a truncated, non-functional protein during translation (62,63). The deficit in functional CLCN1 causes the sarcolemma to become hyperexcitable, thereby increasing its susceptibility to myotonic discharges that impair muscle fiber relaxation (59,62,64). The correction of *Clcn1* missplicing by various therapeutic interventions has been associated with improvements in myotonia in the HSA^{LR} mouse model of DM1 (64–66).

Other examples of adverse ASEs in DM1 that are associated with skeletal muscle dysfunction include the missplicing of the sarcoplasmic/endoplasmic reticulum calcium ATPase 1 (*ATP2A1*; exon 22), ryanodine receptor 1 (*RYR1*; exon 70), and bridging integrator 1 (*BIN1*; exon 11) mRNA transcripts, whose protein products have integral roles in EC coupling and relaxation mechanisms (56,67–69). RYR1 regulates the release of calcium from the sarcoplasmic reticulum, a process that is required for muscle fiber contraction (68,70). In contrast, ATP2A1 (also known as SERCA1) enables the re-uptake of calcium into the sarcoplasmic reticulum during muscle fiber relaxation (70). BIN1 proteins contribute to the structural integrity and formation of the T tubule network on which EC coupling is highly dependent (69). Collectively, these proteins mediate the dynamic processes that generate skeletal muscle force and facilitate movement. Thus, splicing defects in ATP2A1, RYR1 and BIN1 mRNA transcripts have been postulated to contribute to DM1-associated skeletal muscle weakness and wasting (56,67,68).

In addition to those described, multiple DM1 ASEs in skeletal muscle have been linked to ultrastructural abnormalities, contractile weakness, and signaling perturbations (outlined in **Table 2**) (34,38,56,58,71–73). Recent work has shown that the combined effects of these splicing perturbations can underlie pathological features in the skeletal muscles of DM1 mice (74). However, the functional impact(s) of the vast majority of identified DM1 ASEs remain

uncharacterized (56,57). Nevertheless, splicing defects that correlate with or directly influence the DM1 skeletal muscle phenotype can serve as important markers of disease progression and help evaluate the efficacy of therapeutic interventions (56).

.**Table 2.** Select examples of DM1 ASEs in skeletal muscle.

Gene Product	ΔASE	Associated or Postulated Impairment(s)	Reference(s)
Muscle-specific chloride channel 1 (CLCN1)	ΔExon 7A	Myotonia	(59,60)
Sarco/endoplasmic reticulum calcium ATPase 1 (ATP2A1)	ΔExon 22	Altered Ca^{2+} homeostasis	(67)
Bridging integrator 1 (BIN1)	ΔExon 11	Altered T-tubule formation Skeletal muscle weakness	(69)
Ryanodine receptor 1 (RYR1)	ΔExon 70	Altered Ca^{2+} homeostasis and EC coupling	(67,68)
Fast troponin T (TNNT3)	ΔFetal Exon	Altered sarcomere structure	(34)
LIM domain binding 3 (LDB3)	ΔExon 11	Altered sarcomere structure CELF1 upregulation	(73)
$Ca_v1.1$ voltage-dependent calcium channel (CACNA1S)	ΔExon 29	Altered Ca^{2+} regulation and EC coupling Skeletal muscle weakness	(72)
Pyruvate kinase M2 (PKM2)	ΔExon 10	Altered energy metabolism	(71)
Calcium/calmodulin-dependent protein kinase II **(**CAMK2B)	ΔExon 13	Signaling perturbations	(56,75)
Insulin receptor (INSR)	ΔExon 11	Insulin resistance	(38)

1.2.3 Altered Signaling Pathways in DM1 Skeletal Muscle

Despite the historical focus on studying the molecular pathology and its impact in skeletal muscle, the plethora of cellular dysfunctions observed in DM1 also includes perturbations across multiple signaling axes. Indeed, alterations in the activity of several pathways regulated by glycogen synthase kinase 3β (GSK3β) (76), TWEAK/Fn14 (77), mammalian target of rapamycin complex 1 (mTORC1) (75,78), and AMP-activated protein kinase (AMPK) (75,79) have more recently emerged as key contributors to the DM1 skeletal muscle phenotype, and are associated with disease features to varying extents. The increased activity of GSK3β is linked to impairments in muscle fiber regeneration that contribute to progressive skeletal muscle weakness (76). Similarly, the upregulation of TWEAK/Fn14 signaling, has been suggested to promote muscle fiber degeneration in DM1 (77). Metabolic dysfunction in HSA^{LR} mice and DM1 patient muscle cells have been shown to arise from the abnormal signaling responses of key metabolic proteins, mTORC1 and AMPK (75), the latter of which was discovered by the Jasmin Laboratory to be markedly repressed in DM1 skeletal muscle (79). Moreover, several studies have indicated that CUG^{exp} RNA foci expression (36,76) and concomitant splicing abnormalities (56,71,75) can cause or exacerbate dysregulated signaling in DM1; however, the underlying molecular mechanism(s) for most of these perturbations remain unclear.

Given the significant influence of these proteins in skeletal muscle physiology, the modulation of their respective signaling axes is emerging as a promising therapeutic strategy for DM1. Indeed, genetic or pharmacological interventions targeting GSK3β, TWEAK/Fn14, mTORC1, or AMPK signaling in preclinical models have been shown to ameliorate several characteristics of DM1 skeletal muscle including myotonia, muscle weakness, nuclear CUG^{exp} RNA foci accumulation, aberrant alternative splicing, and histopathology (75–77,79,80). In line

with our previous work on altered signaling pathways in DM1 (79,81), a central research aim of the Jasmin Laboratory focuses on the impact of AMPK as a therapeutic target in DM1 skeletal muscle.

1.3 AMP-Activated Protein Kinase

Cellular functions primarily depend on the availability of chemical energy sourced from adenosine triphosphate (ATP) molecules, which are hydrolyzed to release energy and subsequently form adenosine diphosphate (ADP) or monophosphate (AMP). The regulation of metabolism, which encompasses the various processes by which energy is produced and expended in the cell, involves the monitoring and maintenance of the intracellular supply of ATP under a variety of physiological conditions (82). AMP-activated protein kinase (AMPK) is a master regulator of energy homeostasis that mediates metabolic adaptations in response to reduced ATP availability.

The heterotrimeric AMPK complex is composed of an α, β, and γ subunit that each have distinct roles in its structure, function, and activity (83) (**Figure 2**). The α subunit is catalytic, while the non-catalytic β and γ subunits are regulatory with specific involvement in scaffolding and nucleotide-binding, respectively (84–87). The potential combinations of the subunit isoforms (α1 or α2; β1 or β2; γ1, γ2 or γ3) give rise to twelve different AMPK isoenzymes, several of which have been shown to be expressed in a tissue-specific manner (88,89).

AMPK is activated under physiological conditions that increase the cellular AMP to ATP ratio, such nutrient deprivation and exercise (90–92). The activation of AMPK involves two canonical mechanisms: [1] upstream phosphorylation of the catalytic α subunit at threonine-172 (Thr172) by the constitutively active liver kinase B1 (LKB1) (93,94), and [2] binding of AMP to the regulatory γ subunit (92). In particular, AMP binding allosterically activates AMPK, further promotes Thr172 phosphorylation by LKB1, and protects against phosphatase-mediated

dephosphorylation, thereby increasing net AMPK activation (95,96). AMP itself can modestly activate AMPK (96); however, Thr172 phosphorylation is additionally required for maximal enzymatic activity (97,98). While LKB1 is the major upstream kinase that regulates AMPK activation, calcium/calmodulin-dependant protein kinase kinase β (CaMKKβ) has also been shown to phosphorylate AMPK at Thr172 in response to increased intracellular Ca^{2+}, without changes in AMP levels (92,99).

In addition to physiological stimuli, a variety of compounds have been identified as pharmacological AMPK agonists including 5-aminoimidazole-4-carboximide ribonucleotide (AICAR), metformin, and several small molecule activators (100–105). AICAR (also known as ZMP) is an AMP mimetic that similarly binds to the γ subunit and stimulates both allosteric activation and upstream Thr172 phosphorylation of AMPK, albeit to a lesser extent than AMP (98,102). Metformin, an indirect AMPK activator, has been suggested to increase the ratio of cellular AMP to ATP by inhibiting complex I of the mitochondrial electron transport chain (106,107). In contrast to the activation mechanisms of AICAR and metformin, small molecule AMPK agonists have been shown to directly bind to the allosteric drug and metabolite (ADaM) site, located between the α and β subunits of the AMPK complex (108), which allosterically activates AMPK and protects against Thr172 dephosphorylation (100,104).

Once activated, AMPK coordinates the inhibition of anabolic processes (e.g., protein synthesis) while stimulating catabolic processes (e.g., glycolysis) to produce ATP and restore cellular energy homeostasis (109). Acute and chronic metabolic adaptations elicited by AMPK activation are mediated by its interactions with various substrates, including acetyl-coA carboxylase (ACC), another metabolic enzyme whose phosphorylation by AMPK is a classical marker of AMPK activity (91). Indeed, the AMPK signaling network comprises over a hundred

downstream targets and subsequently influences a diverse range of cellular functions (109), thereby establishing AMPK as a prime molecular candidate for study in a variety of biological contexts, including disease.

1.3.1 AMPK-Mediated Skeletal Muscle Adaptations

In addition to its role as a cellular energy sensor, AMPK is also an important regulator of skeletal muscle plasticity. In particular, AMPK has been shown to mediate structural and functional adaptations in skeletal muscle through its coordination of various cellular processes, including metabolism, protein synthesis, and autophagy (110). A well-established effect of long-term pharmacological or exercise-induced AMPK activation is the promotion of a more oxidative phenotype that is characterized by increased mitochondrial content, a shift in muscle fiber type composition from fast-twitch type II to slow-twitch type I muscle fibers, and enhanced endurance capacity (111–114). These metabolic adaptations involve the AMPK-mediated increase in the expression of peroxisome proliferator-activated receptor gamma coactivator-1 alpha (PGC1α), a master regulator of mitochondrial biogenesis and downstream target of AMPK (115). AMPK is also implicated in the regulation of skeletal muscle structure and mass via its regulation of the anabolic and catabolic processes of protein synthesis and autophagy, respectively (116). AICAR-induced AMPK activation has been shown to inhibit the activity of mTORC1, a key regulator of protein synthesis (117), and stimulates the induction of autophagy (118). Perturbations in these major cellular processes have been suggested to underlie skeletal muscle impairments and dysfunction (119,120). For this reason, AMPK has been implicated as a therapeutic target for several neuromuscular diseases, including DM1, in which the effects of its chronic activation have been shown to be beneficial (121).

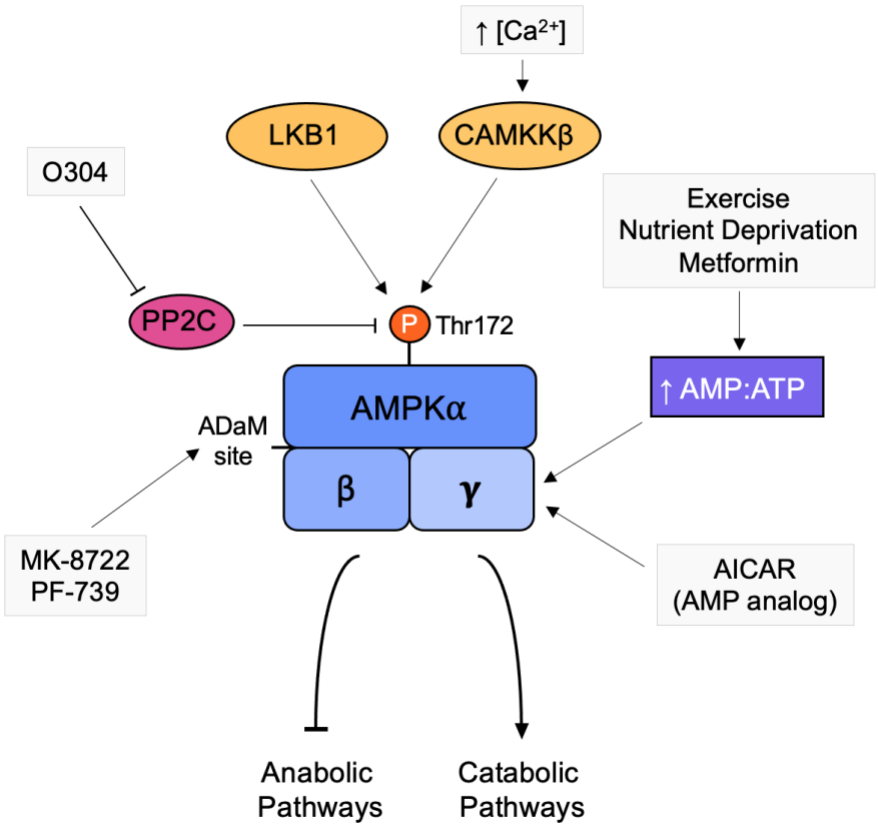

Figure 2. The heterotrimeric AMPK complex and selected mechanisms of its activation. AMPK is comprised of an α, β, and γ subunit and canonically activated by upstream phosphorylation and allosteric binding of AMP to the γ subunit. The catalytic α subunit is phosphorylated at Thr172 by the upstream kinases LKB1 or CAMKKβ, the latter of which is stimulated by increased Ca^{2+} levels. An increase in the cellular ratio of AMP to ATP caused by physiological conditions (e.g., exercise or nutrient deprivation) or pharmacological compounds (e.g., metformin) stimulates AMPK activation. Pharmacological agonists of AMPK also include the AMP-mimetic AICAR, ADaM site-binding small molecules (MK-8722 and PF-739), and O304, which prevents the dephosphorylation of AMPK by protein phosphatase 2C (PP2C). Once activated, AMPK mediates the restoration of energy homeostasis by inhibiting anabolic pathways and promoting catabolism.

1.4 Therapeutic Potential of AMPK in DM1 Skeletal Muscle

Within the past decade, AMPK has emerged as a promising therapeutic target for DM1 after its chronic activation was first shown by the Jasmin Laboratory to be an effective therapeutic approach for Duchenne muscular dystrophy (DMD) (122–125). A wide range of pharmacological and physiological interventions that stimulate AMPK activation have now collectively revealed its beneficial effects also on the DM1 skeletal muscle phenotype. Laustriat *et al*. (126) initially demonstrated that metformin treatment reverses the missplicing of several mRNAs, including *ATP2A1* (exon 22), *TNNT2* (exon 5) and *INSR* (exon 11), in primary myoblasts from DM1 patients. The authors also reported that treatment with AICAR elicited similar improvements in *TNNT2* and *ATP2A1* splicing perturbations, thereby providing preliminary evidence for a partial role for AMPK in correcting DM1 ASEs.

Subsequent work by Brockhoff *et al*. (75) revealed that AMPK signaling is dysregulated in the HSA^{LR} mouse model of DM1. In particular, the activation of AMPK and downstream induction of autophagy were shown to be impaired in response to nutrient deprivation in the tibialis anterior (TA) muscles of 2-month-old HSA^{LR} mice. The lack of increase in Thr172-phosphorylated AMPK levels was independent of LKB1 protein abundance, which did not significantly differ between HSA^{LR} and control mice irrespective of experimental conditions. Similar observations were reported in transdifferentiated muscle cells from DM1 patients, which displayed a comparatively mild induction of autophagy in response to glucose deprivation. The dysregulation of AMPK, whose signaling axis is interlinked with that of mTORC (127), was accompanied by the abnormal activation of downstream targets of mTORC1, but not mTORC1 itself, under fasted conditions in both DM1 mouse and patient muscles.

In contrast to findings from Laustriat *et al*. (126), Brockhoff *et al*. demonstrated that short-term (1-week) treatment with AICAR, but not metformin, reduced myotonia, *Clcn1* exon 7A missplicing, and the nuclear accumulation of CUG^{exp} RNA foci in HSA^{LR} mice. Interestingly, AICAR mitigated several DM1 skeletal muscle features in comparison to the mTORC1 inhibitor rapamycin, which improved myotonic symptoms independent of changes in CUG^{exp} RNA foci accumulation or DM1 ASEs (75). These results further established a therapeutic role for AMPK in DM1 skeletal muscle and shed light on a potential mechanism involving the dispersion of CUG^{exp} RNA foci, in addition to the regulation of alternative splicing processes.

Complementary findings from the Jasmin Laboratory (79) further revealed that the levels of phosphorylated AMPK and PGC1α are significantly reduced in the extensor digitorum longus (EDL) muscles of 9-month-old HSA^{LR} mice, without changes in total AMPK protein abundance. In line with results from Brockhoff *et al*. (75), Ravel-Chapuis *et al*. demonstrated that a 6-week treatment with AICAR reduced nuclear CUG^{exp} RNA foci accumulation and corrected *Atp2a1, Ryr1, Tnnt3* and *Clcn1* DM1 ASEs in the EDL muscles of HSA^{LR} mice, thereby confirming the beneficial effects of AICAR-induced AMPK activation in DM1 skeletal muscle. Moreover, the extended treatment with AICAR elicited additional improvements in histopathological abnormalities and induced a more oxidative phenotype in HSA^{LR} mouse muscles. Importantly, the beneficial effects of AICAR on DM1 ASEs and nuclear CUG^{exp} RNA foci dispersion were also recapitulated in transdifferentiated muscle cells from DM1 patients (79).

In addition to pharmacological AMPK activation, Ravel-Chapuis *et al*. further examined the effect of physiological AMPK activation in DM1 skeletal muscle by initiating a therapeutic approach with exercise. With these experiments, our lab discovered that several weeks of volitional wheel running improved the DM1 skeletal muscle spliceopathy in 4–8-month-old HSA^{LR} mouse

muscles (79). Subsequent reports from Manta *et al*. (65) and Sharp *et al*. (128) confirmed the beneficial impact of exercise on DM1 ASEs in HSA^{LR} mice, and revealed additional improvements in CUG^{exp} RNA foci accumulation, MBNL1 sequestration, myotonia, and skeletal muscle function in response to wheel running and treadmill exercise interventions. Although the acute activation status of AMPK was not evaluated in the aforementioned studies, recent work from Mikhail *et al*. (129) demonstrated that AMPK activation is significantly increased following a single bout of treadmill exercise in HSA^{LR} mice. Similar observations were reported in DM1 patient muscle biopsies, which displayed lower baseline levels of Thr172-phosphorylated AMPK that trended towards an increase in response to chronic exercise in a recent clinical study (130). These results suggest that exercise, unlike prolonged nutrient deprivation (75), is capable of stimulating AMPK activation in DM1 skeletal muscle and can elicit beneficial adaptations that mitigate key disease features in this tissue.

While the molecular mechanism(s) underlying impaired AMPK signaling in DM1 skeletal muscle remain unknown, the collection of evidence from the aforementioned studies has established the beneficial impact of AMPK activation on the disease pathology. Taken together, these findings have expanded the repertoire of potential DM1 therapeutics to include pharmacological and/or physiological interventions that target AMPK.

1.5 Therapeutic Approaches for DM1

As previously mentioned, there is no cure for DM1 and current clinical recommendations are based on the management of individual symptoms (14). Within the DM1 drug development pipeline are several nucleic acid-based therapies and repurposed small molecules that are progressing through clinical trials at various stages (131). These therapeutic approaches have been shown to target one or more aspects of the disease pathology such as the formation of toxic DMPK

RNA foci, misregulation of RNA-binding proteins, perturbations in cell signaling pathways, and tissue-specific impairments. Potential drug candidates that have recently advanced to phase II or III clinical trials include metformin (AMPK activator), mexiletine (anti-myotonia medication), tideglusib (GSK3β inhibitor), and erythromycin (antibiotic medication) (131,132). In addition to pharmacological interventions, aerobic exercise has also been examined as a potential lifestyle intervention for DM1 that can improve skeletal muscle function (130), although the lack of large-scale studies with standardized exercise parameters and physiological measurements in DM1 patients has hindered its clinical application (133). Moreover, given the highly complex and multisystemic nature of DM1, the efficacy of combinatorial treatment approaches has been previously explored at the preclinical level (66,134,135). This strategy has been shown to mitigate the DM1 skeletal muscle pathology through the combination of synergistic small molecules (66) or nucleic acid-based therapy and exercise (134). As various therapeutic interventions progress through the DM1 pipeline, these findings suggest that their potential combinations might be advantageous for the treatment of this disease and therefore warrant future investigation.

1.6 Rationale & Hypothesis

Given our findings of reduced AMPK activation and the beneficial impacts of AICAR and volitional wheel running exercise on the DM1 skeletal muscle phenotype (79), we sought to determine whether the combination of these AMPK agonists would enhance disease correction in HSA^{LR} mice. A swimming regimen was selected because it is a low impact type of exercise that has been previously shown to have beneficial effects in preclinical disease models displaying skeletal muscle degeneration (136,137), but has not been evaluated in the context of DM1 skeletal muscle to date. The goal of this translational aim is to provide insight into combinatorial therapeutic approaches for DM1 that synergistically or additively activate AMPK and examine the

effect of low-impact aerobic exercise in DM1 skeletal muscle. *We hypothesize that activating AMPK both pharmacologically and physiologically will additively or synergistically mitigate the DM1 pathology in skeletal muscle, and that swimming exercise will elicit similar improvements in the DM1 skeletal muscle phenotype as previously reported in our initial work with wheel running.*

Objectives:

1. Determine if a combinatorial therapeutic approach with daily AICAR treatment and swimming exercise for 4 weeks can potentiate improvements in the DM1 skeletal muscle phenotype in male and female HSA^{LR} mice.
2. Examine the impact of 4 weeks of swimming exercise on the DM1 skeletal muscle phenotype in male and female HSA^{LR} mice.

Chapter 2: Materials & Methods

2.1 Ethics Approval

All procedures and experiments performed in this study were approved by the University of Ottawa Animal Care Committee and met the standards of the Canadian Council on Animal Care and Ontario Animals for Research Act. All mice were housed and cared for by the University of Ottawa Animal Care and Veterinary Service throughout the duration of this study.

2.2 Animal Models & Drug Treatments

Two- to three-month-old male and female wild-type FVB/N (IMSR Cat# JAX:001800, RRID: IMSR_JAX:001800), HSA^{SR}, and DM1 HSA^{LR} mice line LR20b (IMSR Cat# JAX:032031, RRID: IMSR_JAX:032031, obtained from Dr. Charles Thornton, University of Rochester) were used in this study. Age-matched WT and HSA^{SR} (transgenic control expressing five CUG repeats in the 3' UTR of the human skeletal actin transgene) mice were used as untreated, sedentary controls. In line with previous investigations involving AICAR treatment in HSA^{LR} mice (75,79), a sample size of 4-6 mice per experimental group was used. WT and HSA^{SR} mice were pooled into a control (CTL) group. Treatments with AICAR (Toronto Research Chemicals, Toronto, Canada; 500 mg/kg per day, subcutaneous injection) or vehicle (saline) were administered one hour prior to the first bout of exercise and at the same time each day. Food and water were provided *ad libitum*. Eighteen to 24 hours following the last bout of exercise or drug administration, mice were euthanized via pentobarbital injection. To assess long-term adaptations in DM1 skeletal muscle, the EDL, TA, and gastrocnemius muscles were harvested. These muscles were selected for study because they are extensively recruited during swimming exercise (138,139) and are primarily composed of fast-twitch muscle fibers, in which the HSA promotor containing CUG^{exp} repeats is predominantly activated (140,141). Hindlimb skeletal muscles were dissected

and either snap frozen in liquid nitrogen for RNA extraction or embedded in Tissue-Tek OCT compound (VWR, Mississauga, Canada) for histological and immunofluorescence analyses. Since sex is a modifying factor influencing the phenotype in DM1 (142,143), male and female mice were analyzed separately to account for potential differences between sexes.

2.3 Exercise Protocol

The swim tank apparatus was adapted from Evangelista *et al.* (144) and consisted of a large tank (49 cm height, 97.5 cm length, and 57 cm width) divided into 12 swimming zones by a Plexiglas grid. Each zone had a surface area of 15.5 cm by 19.5 cm and an approximate water depth of 20 cm to enable individual exercise. The temperature of the water was maintained between 30-32°C using a portable immersion heater. To prevent mouse inactivity due to flotation, water bubbles were continuously generated by tubes attached to a nitrogen gas cylinder to break water surface tension and encourage constant locomotion. DM1 (HSA^{LR}) mice were acclimated to the swimming protocol by gradually increasing the duration of exercise up to 30 minutes over the course of 3 days. Following acclimation, mice were subjected to 30-minute bouts of swimming twice daily, 5 days per week for a total of 4 weeks. Sedentary control mice (WT and HSA^{SR}) were placed in the tank for 5 minutes twice a week to mimic water stress elicited by the exercise protocol. To avoid significant discomfort or drowning, mice were closely monitored during each bout of exercise and were given a short (1-minute) break or removed from the tank if exhaustion was observed.

2.4 Fluorescent *in situ* Hybridization

Frozen TA skeletal muscle cross-sections (10 µm) were air-dried for 30 minutes at room temperature and fixed in 4% paraformaldehyde in 1X D-PBS (Wisent Bioproducts, Saint-Jean-Baptiste, QC, Canada) for 30 minutes. Sections were permeabilized using 2% acetone (pre-chilled

at -20°C) or 0.5% Triton X-100 in 1X D-PBS for 5 minutes, rehydrated using 1X D-PBS for 10 minutes, and incubated in 30% formamide, 2X UltraPure SSC Buffer (Invitrogen) for 10 minutes at room temperature. Sections were incubated with a Cy3-labelled (CAG)5 oligonucleotide probe (1 ng/µl; Cat#F5001; PNA Bio, Thousand Oaks, California, USA) diluted in FISH buffer (30% formamide, 2X SSC, 0.02% BSA, 66 ug/mL yeast tRNA, 10% dextran sulfate, 2 mM vanadyl ribonucleoside complex) for 2 hours at 37°C, followed by a 30-minute wash in 30% formamide, 2X SSC at 45°C and two 30-minute washes in 1X SSC at room temperature. Finally, sections were mounted with Vectashield Mounting Medium containing DAPI (Vector Laboratories, Burlingame, CA, US). Images of whole skeletal muscle cross-sections were acquired at 20X magnification (0.8 NA; air) and analyzed using Imaris (RRID:SCR_007370). For analysis, three ROIs were randomly selected per cross-section. Imaris Spot Detection functions were used to identify nuclei (as indicated by DAPI) and RNA foci, respectively, and applied to all images. The number of nuclear RNA foci detected by the CAG(5) probe was automatically quantified using the Imaris Colocalization (Object) function and expressed as a percentage of the total number of nuclei identified. The average number of nuclei counted per cross-section was ~1700 and no differences were observed in the total number of nuclei identified between experimental groups (**Fig. A1**).

For co-localization analyses with MBNL1 following FISH staining, muscle cross-sections were thrice washed in 1X D-PBS, blocked with 1% goat serum albumin and 1% BSA in 1X D-PBS for 1 hour at room temperature, and incubated with anti-MBNL1 primary antibody (1:250; Abcam Cat#ab45899, RRID: AB_1310475) overnight at 4°C. After washing with 1X D-PBS, sections were incubated with an Alexa fluorophore 488-conjugated goat anti-rabbit IgG (1:200; ThermoFisher Scientific) secondary antibody, washed with 1X D-PBS, and mounted with Vectashield Mounting Medium containing DAPI (Vector Laboratories). Three randomly selected

ROIs per cross-section were imaged at 63X magnification (1.4 NA; oil) using Z-Stacks (20 focal planes collected at 0.430 μm intervals). All images were analyzed using Imaris Spot Detection functions to identify nuclei (DAPI), RNA foci, and MBNL1 puncta. For MBNL1, the same fluorescence intensity threshold was applied to each image to detect MBNL1 puncta. The number of MBNL1 puncta that co-localized with nuclear RNA foci was automatically measured and expressed as a percentage of the total number of nuclei identified (an average of ~70 ± 11 nuclei per ROI).

2.5 RT-PCR

Total RNA was extracted from skeletal muscle tissue by homogenizing muscle powder in TRIzol reagent (Roche). Samples were shaken for 15 minutes with 200 μl of chloroform and centrifuged at 13,000 rpm for 15 minutes at 4°C. The clear aqueous phase containing RNA was collected and purified by treatment with DNase (Invitrogen/ThermoFisher Scientific). For reverse transcription, 500 ng to 1 μg of RNA was used to synthesize cDNA with RT Master Mix (abm G490). RT-PCR was performed using GoTaq Flexi DNA polymerase (Promega) and mouse primers for *Atp2a1* exon 22, *Ryr1* exon 70, *Clcn1* exon 7a, and *Bin1* exon 11 DM1 alternative splicing events (**Table 3**). RT-PCR products were run on 5% acrylamide gels, stained with GelRed dye (Biotium, Freemont, California), and imaged using a Gel Doc XR+ Imaging System (Bio-Rad, Hercules, CA, US). Quantification of alternative splicing patterns (% of exon inclusion or exclusion) was determined using ImageLab (Bio-Rad) software (Image Lab Software, RRID:SCR_014210) by measuring the ratio between the respective band intensities of fetal and adult splicing isoforms.

2.6 Central Nucleation Analyses

Skeletal muscle cross-sections (10 μm) were stained with hematoxylin and eosin (H&E), washed with subsequent ethanol solutions (70%, 90% and 100%), and mounted with toluene. Images of whole muscle cross-sections were acquired at 10X magnification (0.45 NA; air). For TA muscle cross-sections, images were acquired at 20X magnification (0.8 NA; air). For central nucleation analyses, three ROIs per muscle cross-section were randomly selected for analysis. The number of centrally located nuclei were visually counted and expressed relative to the total number of nuclei.

2.7 Muscle Fiber Cross-Sectional Area Analyses

Skeletal muscle cross-sections were immunostained with a laminin-specific primary antibody (**Table 4**) and mounted with Vectashield Mounting Medium containing DAPI. Cross-sections were imaged at 20X magnification (0.8 NA; air). For EDL muscles, the CSA of individual myofibers within an entire cross-section was analyzed. For TA muscles, three ROIs were randomly selected for analysis. The CSA of individual myofibers was measured using Cellpose (145) and the LabelsToROIs ImageJ plugin (146).

2.8 Western Blotting

Whole skeletal muscles were crushed on dry ice, and muscle powder was resuspended and homogenized in urea buffer (7 M urea, 2 M thiourea, 65 mM CHAPS, 100 mM DTT, 125 mM Tris-HCl pH 6.8, phosphatase and protease inhibitors [PhosSTOP and cOmplete, respectively; Roche]). Protein extracts were centrifuged at 20,000 *g* for 15 minutes at 4°C, and supernatants were collected and stored at -80°C. Skeletal muscle protein concentration was quantified using the CB-X Protein Assay Kit (G-Bioscience, St. Louis, MO). SDS-PAGE was used to separate proteins

(15 to 20 μg), followed by transference onto a nitrocellulose membrane (Amersham Protran 0.2 μm, Cytiva) overnight at 4°C. Equal loading of protein was determined by staining membranes with Ponceau solution (Sigma). Membranes were blocked with 5% skim milk or bovine serum albumin (BSA; Sigma-Aldrich) in 1X PBS-T or TBS-T (phosphate- or Tris-buffered saline containing 1% Tween-20, respectively) followed by incubation with primary antibodies as per manufacturer recommendations (**Table 4**). After washing with 1X PBS-T or TBS-T, incubation with appropriate horseradish peroxidase (HRP)-conjugated secondary antibodies (Jackson Laboratories), and subsequent washing, enhanced chemiluminescence (ECL) reagents (ThermoFisher Scientific) were applied to membranes and bands were visualized using X-ray film (Diamed). Quantification of protein expression levels normalized to Ponceau staining was determined using Bio-Rad Image Lab (Image Lab Software, RRID:SCR_014210) and ImageJ (ImageJ, RRID:SCR_003070) software.

2.9 Succinate Dehydrogenase Staining

Skeletal muscle (TA) cross-sections (10 μm) were incubated with staining medium (1.5 mM nitroblue tetrazolium chloride, 130 mM sodium succinate and 0.1 M PBS pH 7.4) for 1 hour at 37°C and mounted using FluorSave Reagent (Calbiochem, San Diego, CA, USA). Images of whole muscle cross-sections were acquired at 10X magnification (0.45 NA; air) and analyzed using Fiji (Fiji, RRID:SCR_002285). The area of stained fibers at a given intensity (dark, medium, or light) was measured using the same threshold parameters for each image and expressed relative to the total area of the whole muscle section.

2.10 Muscle Fiber Typing

Frozen skeletal muscle cross-sections (10 μm) were air dried at room temperature for 15 minutes and prepared using the M.O.M. Immunodetection Kit (Vector Laboratories). Sections were incubated with MHC type I-, IIA-, and IIB-specific primary antibodies as well as anti-laminin primary antibody (**Table 4**) for 45 minutes at 37°C. Following washes with 1X PBS, sections were incubated with fluorophore-conjugated secondary goat anti-mouse antibodies (**Table 4**) for 30 minutes at 37°C, subsequently washed with 1X PBS, and mounted using FluorSave Reagent (Calbiochem, San Diego, CA, USA). Images of muscle sections were acquired at 20X magnification (0.8 NA; air). Three ROIs per cross-section (~300 muscle fibers per ROI) were randomly selected for analysis of TA muscles. The number of MHC I-, IIA, IIX-, and IIB-positive myofibers were counted and expressed as a percentage of the total number of muscle fibers.

2.11 Image Acquisition

Images were acquired using a Zeiss-AxioImager.M2 microscope with the following objectives: Zeiss 63X Plan-Apochromat (1.4 NA; oil), Zeiss 40X EC Plan-NeoFluar (1.3 NA; oil), 20X Plan-Apochromat (0.8 NA; air), 10X Plan-Apochromat (0.45 NA; air), and 5X EC Plan-NeoFluar (0.16 NA; air). Images of H&E-stained TA cross-sections were acquired using a Zeiss-AxioScan.Z1 microscope with the following objective: 20X Plan-Apochromat (0.8 NA; air). An X-Cite 110 LED lamp (Excelitas Technologies, Vaudreuil, Quebec, Canada) and transmitted LED light source were used for epifluorescence and Brightfield imaging, respectively. Images were acquired and processed using Zeiss AxioCam mRm CCD (monochrome), AxioCam mRc (color) or Hitachi-HV-F202SCL (color) detectors and Zen Blue 2.3 software (ZEN Digital Imaging for Light Microscopy, RRID:SCR_013672).

2.12 Statistical Analysis

One-way ANOVA followed by Tukey's post-hoc test was used to determine if differences between experimental groups were statistically significant. Error bars correspond to the standard error of the mean (SEM). The level of significance was set at $P < 0.05$. GraphPad Prism 9 (GraphPad Prism, RRID:SCR_002798) was used for statistical analysis.

Table 3. Primer sequences used for RT-PCR analyses in this study.

Gene	Species	PCR Primer Sequence 5' → 3'
Atp2a1	Mouse	Forward: ATCTTCAAGCTCCGGGCCCT Reverse: CAGCTTTGGCTGAAGATGCA
Ryr1	Mouse	Forward: GACAATAAGAGCAAAATGGC Reverse: CTTGGTGCGTTCCTGATCTG
Clcn1	Mouse	Forward: GGAATACCTCACACTCAAGGCC Reverse: CACGGAACACAAAGGCACTGAATGT
Bin1	Mouse	Forward: TCAATGATGTCCTGGTCAGC Reverse: GCTCATGGTTCACTCTGATC

Table 4. Antibodies used for Western blot (WB) and immunofluorescence (IF) analyses.

Antibody	Concentration	Reference
PGC1α	WB 1:1000	Abcam Cat#ab54481 RRID: AB_881987
OXPHOS total rodent WB cocktail	WB 1:1000	Abcam Cat#ab110413 RRID: AB_2629281
GAPDH HRP-conjugated	WB 1:2000	Abcam Cat#ab9482 RRID: AB_307272
MBNL1	IF 1:250	Abcam Cat#ab45899, RRID: AB_1310475
Laminin	IF 1:100	Sigma-Aldrich Cat#L9393, RRID: AB_477163
MHC-I BA-D5-supernatant (mouse IgG2b)	IF 1:100	DHSB Cat#BA-D5, RRID: AB_2235587
MHC-IIA SC-71-supernatant (mouse IgG1)	IF 1:100	DSHB Cat#SC-71, RRID: AB_2147165
MHC-IIB BF-F3-purified (mouse IgM)	IF 1:100	DSHB Cat#BF-F3, RRID: AB_2266724
Goat anti-mouse IgG1 A488	IF 1:200	Thermo Fischer Scientific Cat# A-21121, RRID: AB_2535764
Goat anti-mouse IgM A594	IF 1:200	Thermo Fischer Scientific Cat# A-21044, RRID: AB_2535812
Goat anti-rabbit IgG A647	IF 1:200	Thermo Fischer Scientific Cat# A-21044, RRID: AB_2535812
Goat anti-mouse IgG2b CF405	IF 1:200	Millipore Sigma Cat#SAB4600477

Chapter 3: Results

3.1 Introduction

Two- to three-month-old male and female HSA^{LR} mice (hereafter referred to as DM1 mice), which express 250 CTG repeats in the 3'UTR of the human skeletal actin transgene (51), were randomly sorted into sedentary or exercised groups and treated daily with AICAR or saline for 4 weeks. Untreated, sedentary, wild-type (WT) and HSA^{SR} (transgenic model expressing five CUG repeats) mice were used as healthy controls (**Fig. 3**). Following a brief period of acclimation, exercised mice underwent 30-minute bouts of swimming twice daily for five consecutive days per week during the 4-week study (**Fig. 3**).

3.2 Combinatorial treatment with exercise and AICAR additively mitigates nuclear CUG^{exp} RNA foci accumulation in female DM1 mice.

The pathologic formation and nuclear aggregation of CUG^{exp} DMPK mRNA underlies the RNA toxicity model of DM1 (28–30). Previous results have shown that treatment with AICAR or daily exercise reduces the nuclear accumulation of toxic CUG^{exp}-containing mRNA in DM1 skeletal muscles (65,75,79). To determine whether a combinatorial treatment potentiates this effect in DM1 mice, we performed fluorescent *in situ* hybridization (FISH) analyses on TA skeletal muscle cross-sections using a (CAG)5 Cy3-labeled oligonucleotide probe (**Fig. 4A, 5A**). Nuclei were visualized by co-staining the muscle cross-sections with 4′,6-diamidino-2-phenylindole (DAPI). We determined the percentage of CUG^{exp} foci-positive nuclei by colocalization analysis of fluorescent signals (**Fig. 4C, 5C**).

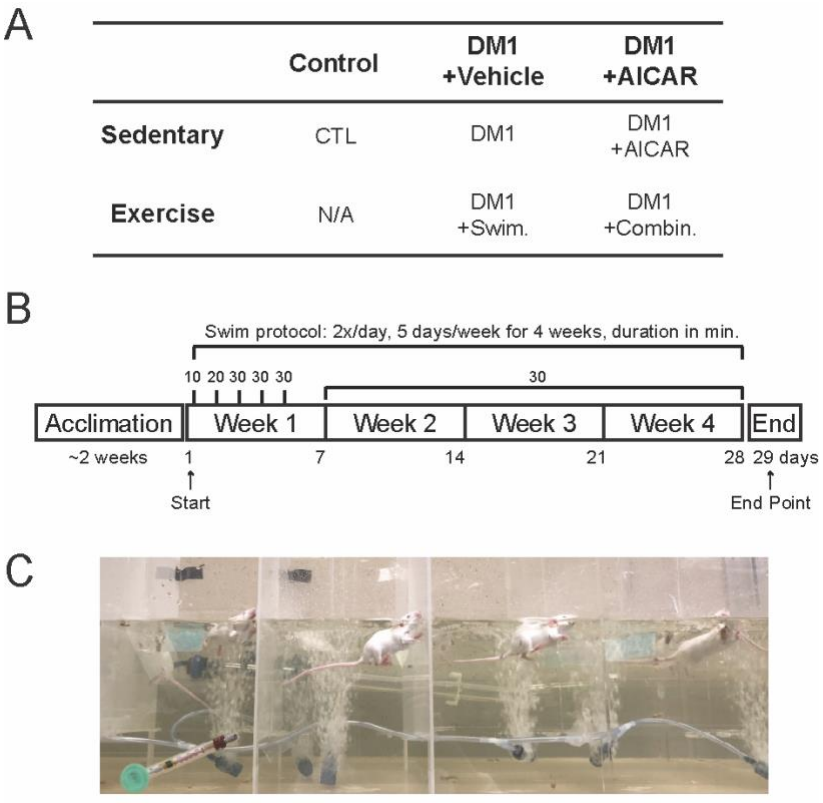

Figure 3. Combinatorial treatment with exercise and AICAR in DM1 mice. (**A**) DM1 mice were treated with saline (DM1), exercised (DM1 + Swim.), treated with AICAR (DM1 + AICAR), or exercised and treated with AICAR (DM1 + Combin.). Wild-type FVB/N and HSA^{SR} mice were used as controls (CTL). (**B**) Timeline of the exercise regimen. (**C**) Swimming apparatus.

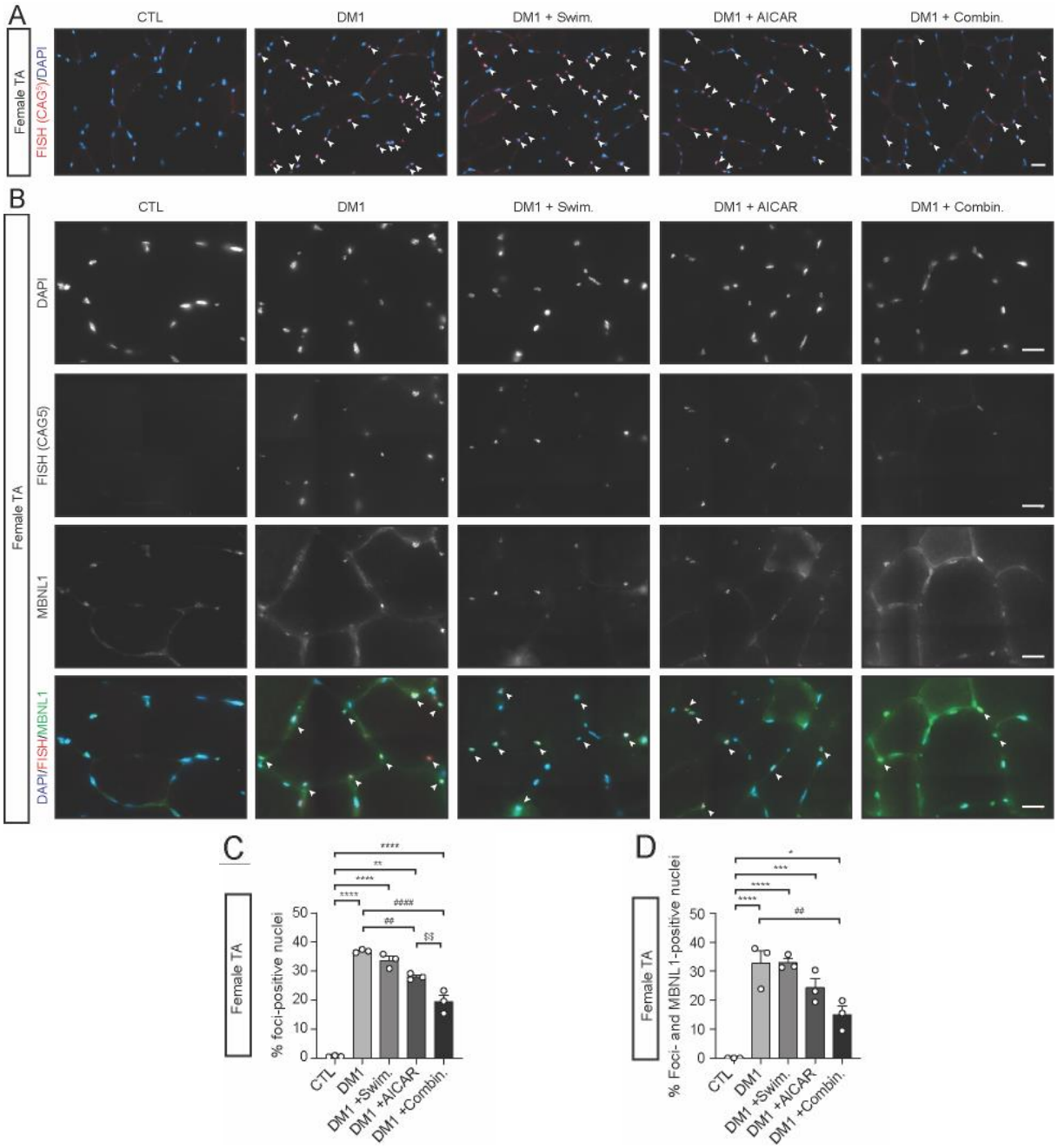

Figure 4. Combinatorial treatment with exercise and AICAR reduces the nuclear accumulation of toxic RNA foci and MBNL1 sequestration in female DM1 mouse TA muscles. (A) Representative FISH staining of female TA muscles. Colocalization of nuclei (blue) and CUG^{exp} RNA foci (red) are indicated by arrows. (**B**) Representative FISH and MBNL1 IF staining of female TA muscles. Colocalization of nuclei (blue), CUG^{exp} RNA foci (red) and MBNL1 (green) are indicated by arrows. (**C**) Percentage of RNA foci-positive nuclei. (**D**) Percentage of MBNL1 sequestration by CUG^{exp} RNA foci. N = 3. One-way ANOVA was used followed by Tukey's post-hoc test (* $p < 0.05$, ** $p < 0.01$, *** $p < 0.001$, **** $p < 0.0001$ vs. CTL or as indicated; ## $p < 0.01$, ### $p < 0.001$, #### $p < 0.0001$ vs. DM1; $$ $p < 0.01$ vs. DM1+ AICAR). Scale bar = 20 μm.

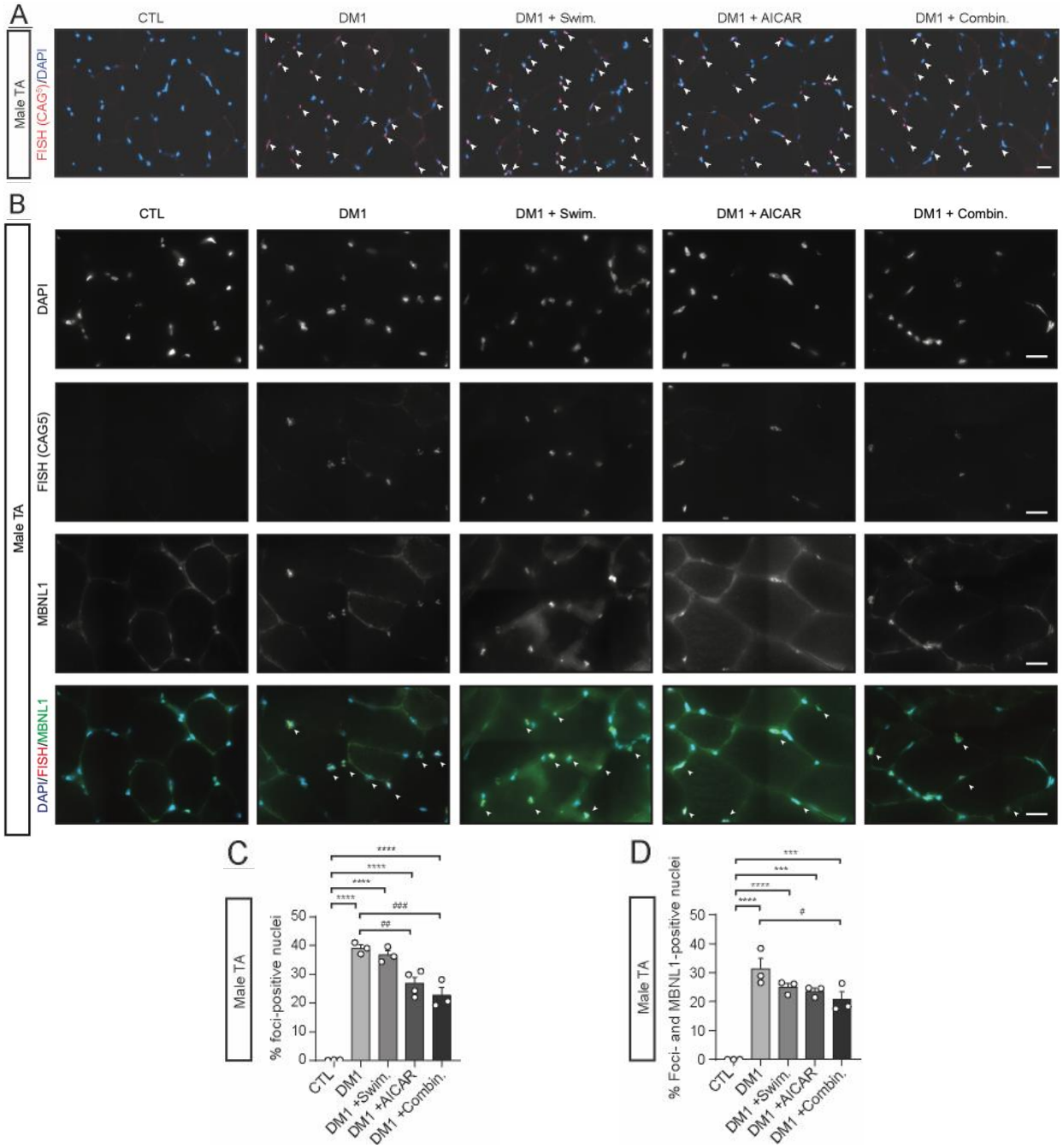

Figure 5. Impact of AICAR treatment and exercise individually and in combination on nuclear RNA foci accumulation and MBNL1 sequestration in male DM1 mouse TA muscles. (**A**) Representative FISH staining of male TA muscles. Colocalization of nuclei (blue) and CUG^{exp} RNA foci (red) are indicated by arrows. (**B**) Representative FISH and MBNL1 IF staining of male TA muscles. Colocalization of nuclei (blue), CUG^{exp} RNA foci (red) and MBNL1 (green) are indicated by arrows. (**C**) Percentage of RNA foci-positive nuclei. (**D**) Percentage of MBNL1 sequestration by CUG^{exp} RNA foci. N = 3-4. One-way ANOVA was used followed by Tukey's post-hoc test (** $p < 0.01$, *** $p < 0.001$, **** $p < 0.0001$ vs. CTL or as indicated; # $p < 0.05$, ## $p < 0.01$, ### $p < 0.001$, #### $p < 0.0001$ vs. DM1). Scale bar = 20 μm.

As expected, no CUG^{exp} foci were detected in the TA muscles of control mice, while approximately ~38% of nuclei were foci-positive in saline treated male and female DM1 mice ($p < 0.0001$) (**Fig. 4C, 5C**). In contrast to the effect of volitional wheel running in DM1 mice (65), we did not observe a significant impact on nuclear foci accumulation following four weeks of swimming exercise alone. AICAR treatment significantly decreased the percentage of foci-positive nuclei by ~30% and ~25% in female (**Fig. 4C**) and male (**Fig. 5C**) DM1 mice ($p < 0.01$ for both sexes), respectively, as previously observed (79). Remarkably, our results demonstrate that the percentage of CUG^{exp} RNA foci-positive nuclei was further reduced (~48%) in combinatorially-treated female DM1 mice as compared to both saline ($p < 0.0001$) and AICAR-treated DM1 mice ($p < 0.01$; **Fig. 4C**). This increased reduction (~42%) was also observed in the TA muscles of combinatorially-treated male DM1 mice ($p < 0.001$ vs. DM1; **Fig. 5C**) but did not significantly differ from AICAR treatment alone.

In addition to nuclear aggregation, CUG^{exp} RNA foci exert a dominant toxic gain-of-function in DM1 by binding and sequestering MBNL1, an important pre-mRNA alternative splicing regulator (30,34,35). The pathological sequestration of MBNL1 by CUG^{exp} in nuclear DMPK mRNA aggregates causes distinct punctate staining (30). Given the marked reduction in nuclear CUG^{exp} RNA foci accumulation observed in the muscles of combinatorially treated DM1 mice, we proceeded to next examine whether a concomitant decrease in MBNL1 sequestration had occurred. As illustrated (**Fig. 4B, 5B**), we performed immunofluorescence (IF) staining with an anti-MBNL1 primary antibody in addition to CAG(5) FISH on TA skeletal muscle cross-sections. The number of MBNL1 puncta, detected using a fluorescence intensity threshold, that co-localized with nuclear CUG^{exp} RNA foci was measured and expressed as a percentage of the total number of nuclei in each image (**Fig. 4D, 5D**). In line with our results of reduced nuclear RNA aggregates,

the number of MBNL1 puncta co-localized to CUG^{exp} foci was significantly decreased in both combinatorially treated male (~34%; $p < 0.05$ vs. DM1) and female (~54%; $p < 0.01$ vs. DM1) DM1 mice (**Fig. 4D, 5D**). Together, our findings reveal that 4 weeks of combinatorial treatment with swimming exercise and AICAR treatment effectively mitigates the nuclear accumulation of RNA foci and concomitant sequestration of MBNL1 in the skeletal muscles of DM1 mice. Our results in female DM1 mice further suggest that swimming exercise potentiates the beneficial effect of AICAR treatment in reducing nuclear CUG^{exp} foci aggregation in comparison to either intervention alone.

3.3 Combinatorial treatment reverses MBNL1-dependent DM1 ASEs in DM1 skeletal muscles with a greater correction observed in female mice.

Prominent symptoms of DM1, including myotonia and skeletal muscle weakness, have been shown to arise from the dysregulation of alternative splicing (59,60,67,69). For any therapeutic intervention to be successful and provide benefits to DM1 muscle, ASEs need to be rescued, ideally even normalized (56). Approximately 80% of DM1 ASEs in skeletal muscle have been attributed to the sequestration and functional inhibition of MBNL1 by toxic RNA foci (47). Given our observations of reduced nuclear CUG^{exp} foci accumulation and MBNL1 sequestration following four weeks of combinatorial treatment, we evaluated whether improvements in the DM1 skeletal muscle spliceopathy had occurred (**Fig. 6, 7**). Using RT-PCR, we analyzed several DM1 ASEs in the TA and gastrocnemius muscles of male and female DM1 mice. In particular, we examined the patterns of MBNL1-dependent splicing targets that are altered in DM1: *Atp2a1* exon 22, *Ryr1* exon 70, *Clcn1* exon 7a, and *Bin1* exon 11 (34,44,48,69) (**Fig. 6, 7**).

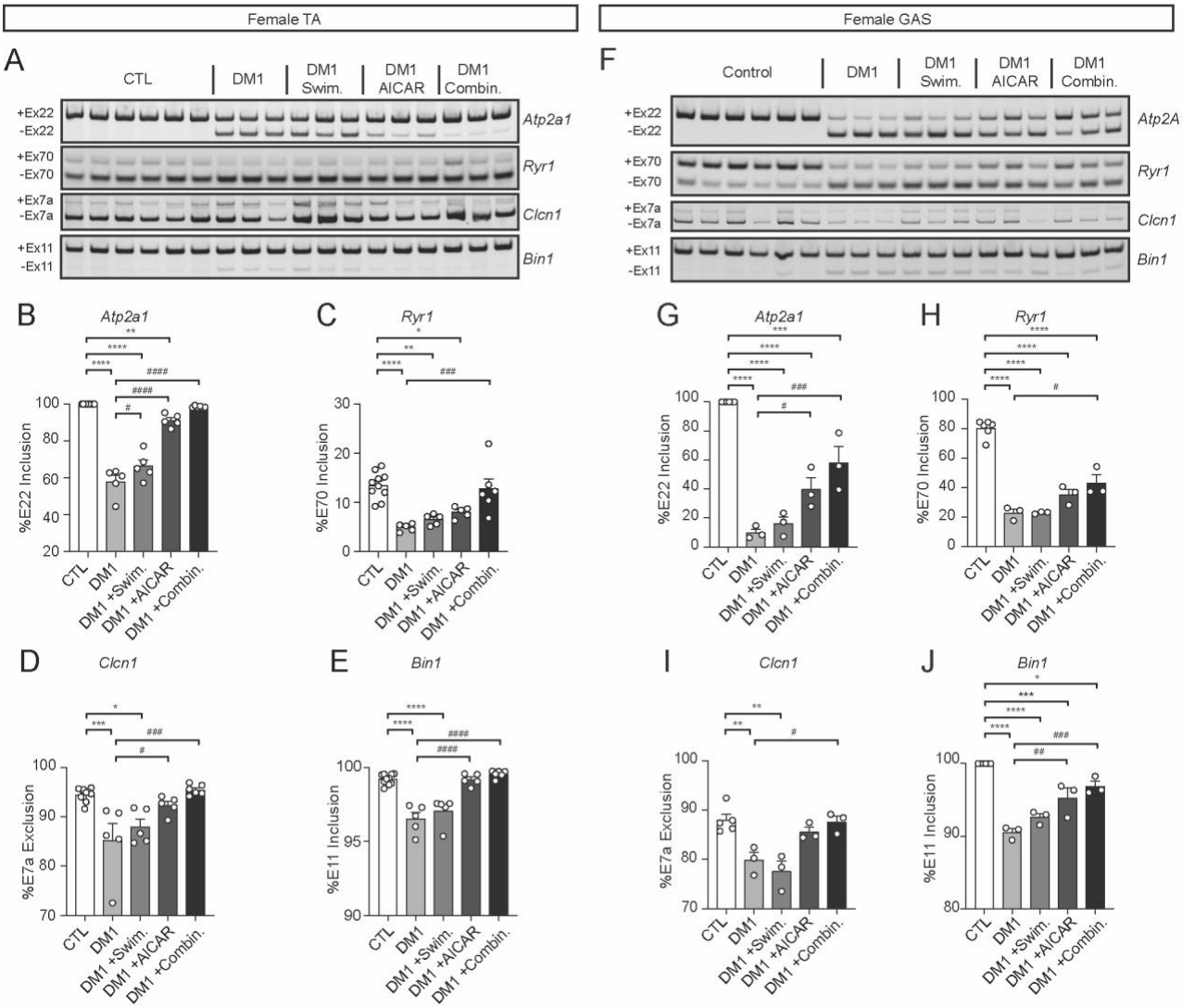

Figure 6. Treatment with AICAR individually and in combination with exercise improves DM1 alternative splicing events in female DM1 mouse skeletal muscles. (**A, F**) Representative RT-PCR analysis showing the splicing patterns of *Atp2a1* exon 22, *Ryr1* exon 70, *Clcn1* exon 7a, and *Bin1* exon 11 in the TA (**A**) and gastrocnemius (**F**) muscles of female control and DM1 mice. (**B-E, G-J**) Percentages of *Atp2a1* exon 22 inclusion, *Ryr1* exon 70 inclusion, *Clcn1* Ex7a exclusion, and *Bin1* exon 11 inclusion with mean ± SEM. N = 3-10. One-way ANOVA was used followed by Tukey's post-hoc test (* $p < 0.05$, ** $p < 0.01$, *** $p < 0.001$, **** $p < 0.0001$ vs. CTL, # $p < 0.05$, ## $p < 0.01$, ### $p < 0.001$, #### $p < 0.0001$ vs. DM1).

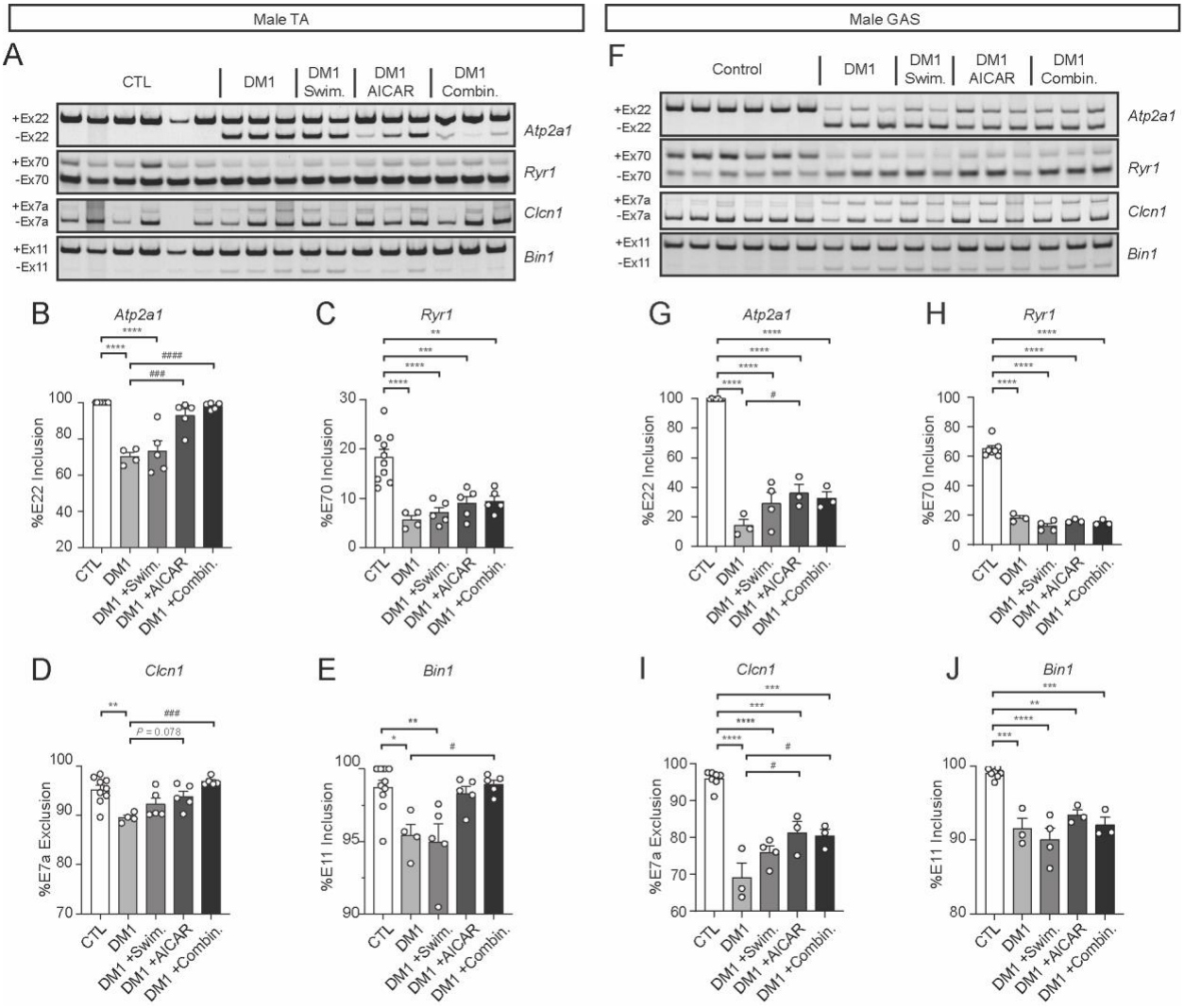

Figure 7. Treatment with AICAR individually and in combination with exercise improves DM1 alternative splicing events in male DM1 mouse skeletal muscles. (**A, F**) Representative RT-PCR analysis showing the splicing patterns of *Atp2a1* exon 22, *RyR1* exon 70, *Clcn1* exon 7a, and *Bin1* exon 11 in the TA (**A**) and gastrocnemius (**F**) muscles of male control and DM1 mice. (**B-E, G-J**) Percentages of *Atp2a1* exon 22 inclusion, *Ryr1* exon 70 inclusion, *Clcn1* Ex7a exclusion, and *Bin1* exon 11 inclusion with mean ± SEM. N = 3-10. One-way ANOVA was used followed by Tukey's post-hoc test (* $p < 0.05$, ** $p < 0.01$, *** $p < 0.001$, **** $p < 0.0001$ vs. CTL, # $p < 0.05$, ## $p < 0.01$, ### $p < 0.001$, #### $p < 0.0001$ vs. DM1).

As previously described, the DM1 splicing patterns of *Atp2a1* exon 22, *Ryr1* exon 70, *Clcn1* exon 7a, and *Bin1* exon 11 result in mRNAs that encode fetal isoforms of these proteins, while the adult splicing isoforms are expressed in healthy tissue (**Fig. 6, 7**). In the TA muscles of female DM1 mice, swimming exercise partially corrected the missplicing of *Atp2a1* exon 22 ($p < 0.05$ vs. DM1), while treatment with AICAR improved *Atp2a1* exon 22, *Clcn1* exon 7a and *Bin1* exon 70 ASEs (**Fig. 6A-E)**. Four weeks of combinatorial treatment elicited a complete rescue in the splicing pattern of all analyzed ASEs in female DM1 TA muscles to the control phenotype (**Fig. 6A-E**). For *Atp2a1* exon 22 and *Ryr1* exon 70 splicing targets, our results are indicative of a trend towards an additive improvement in aberrant alternative splicing following the 4-week combinatorial treatment as compared to AICAR treatment alone ($p = 0.07$ vs. DM1 + AICAR; **Fig. 6A-C**). In female DM1 gastrocnemius muscles, which displayed greater impairments in missplicing (**Fig. 6F-J**), the combinatorial treatment completely rescued *Clcn1* exon 7a and significantly corrected *Ryr1* exon 70 ($p < 0.05$ vs. DM1) ASEs towards the control phenotype in comparison to swimming exercise or AICAR treatment alone.

Similar to our findings in female mice, swimming exercise had only a mild effect on DM1 ASEs in the TA muscles of male DM1 mice, while the combinatorial treatment completely corrected the missplicing of *Atp2a1* exon 22, *Clcn1* exon 7a, and *Bin1* exon 11 ASEs (**Fig. 7A-E**). Beneficial improvements were further observed in male DM1 gastrocnemius muscles as AICAR and the combinatorial treatment partially reversed the missplicing of *Atp2a1* exon 22 and *Clcn1* exon 7a ASEs towards the control phenotype (**Fig. 7F-J**). Unexpectedly, our results showed only a small trend in improvement in *Ryr1* exon 70 missplicing in the TA muscles of AICAR- and combinatorially treated male DM1 mice (**Fig. 7A, C**), while both *Ryr1* exon 70 and *Bin1* exon 11 DM1 ASEs remained unchanged in the gastrocnemius muscles following AICAR or combinatorial

treatment (**Fig. 7F, H**). Given our observations of improved *Ryr1* and *Bin1* missplicing in the muscles of combinatorially treated female DM1 mice, this result may have arisen from sex- or muscle-specific differences in the underlying correction mechanism(s) for these splicing targets in response to the combinatorial treatment. Overall, our findings reveal that four weeks of combinatorial treatment with swimming exercise and AICAR markedly improves the DM1 skeletal muscle spliceopathy for several MBNL1-dependent ASEs, thereby reducing the severity of disease in different types of DM1 mouse muscles. Additionally, our data indicate that these benefits appear to be greater in female DM1 mouse muscles.

3.4 Combinatorial treatment with swimming and AICAR improves the histopathological features of DM1 mouse skeletal muscle and induces hypertrophy in female DM1 mice.

Previous studies have shown that the beneficial effects of AICAR on the DM1 skeletal muscle phenotype are duration-dependant. Indeed, a 1-week treatment with AICAR mitigated RNA toxicity (75), while improvements in both RNA toxicity and muscle histology were observed after 6 weeks of treatment in extensor digitorum longus (EDL) muscles of DM1 mice (79). To examine the impact of the 4-week combinatorial treatment on histological features of DM1 muscles, we performed hematoxylin and eosin (H&E) staining on EDL cross-sections from control and DM1 mice from each experimental group (**Fig. 8A, B**).

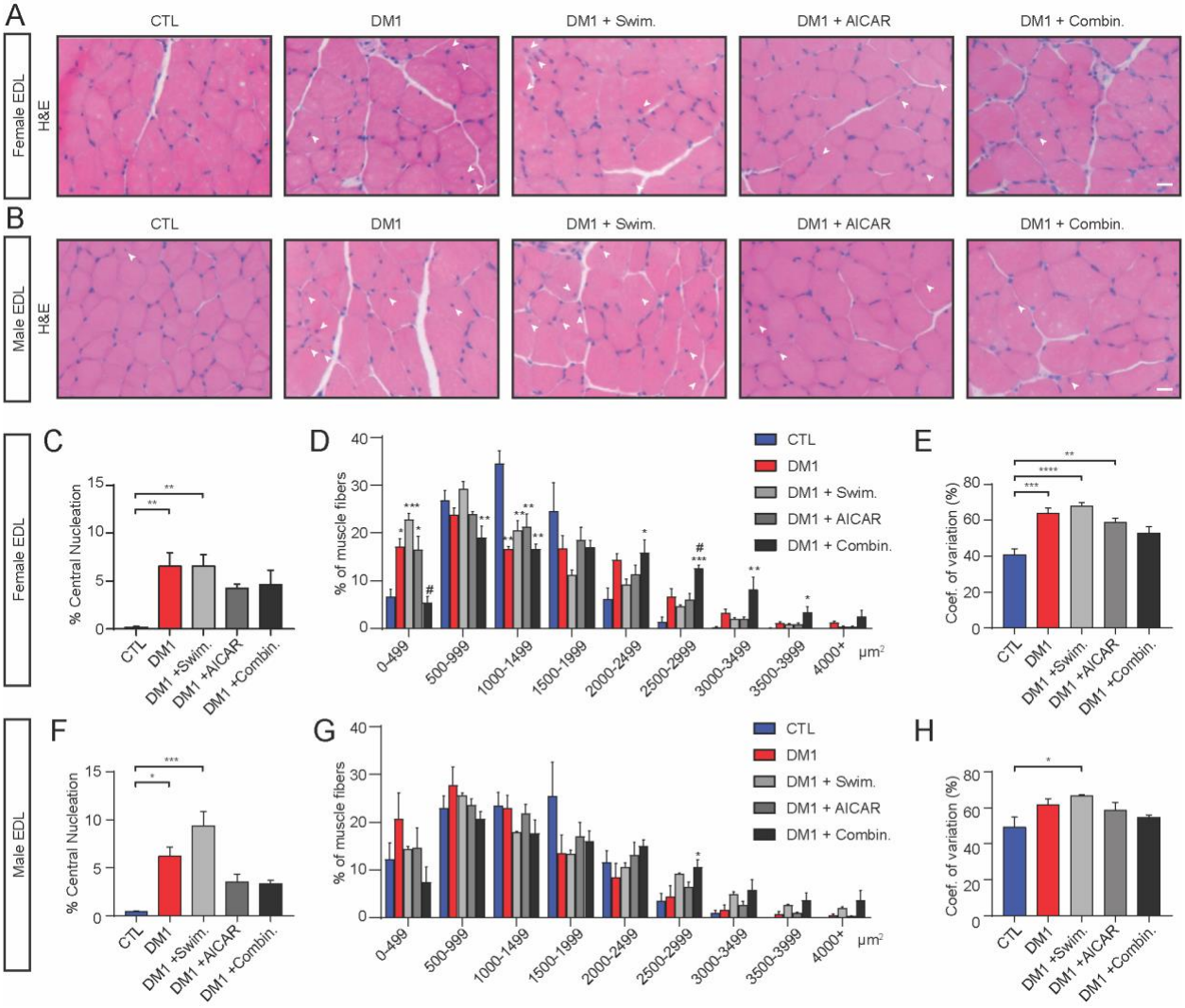

Figure 8. Combinatorial treatment with exercise and AICAR improves the histopathological characteristics of DM1 mouse EDL muscles. (**A, B**) Representative H&E staining of EDL muscles. Centrally located nuclei are indicated by arrows. (**C, F**) Percentages of central nucleation. (**D, G**) EDL myofiber cross-sectional area. **(E, H)** Coefficient of variation of CSA. (**A, C, D, E**) Female EDL muscles, N =3-4 and (**B, F, G, H**) Male EDL muscles, N =3-4. One-way ANOVA was used followed by Tukey's post-hoc test (* $p < 0.05$, ** $p < 0.01$, *** $p < 0.001$, **** $p < 0.0001$ vs. CTL, # $p < 0.05$ vs. DM1). Scale bar = 20 µm.

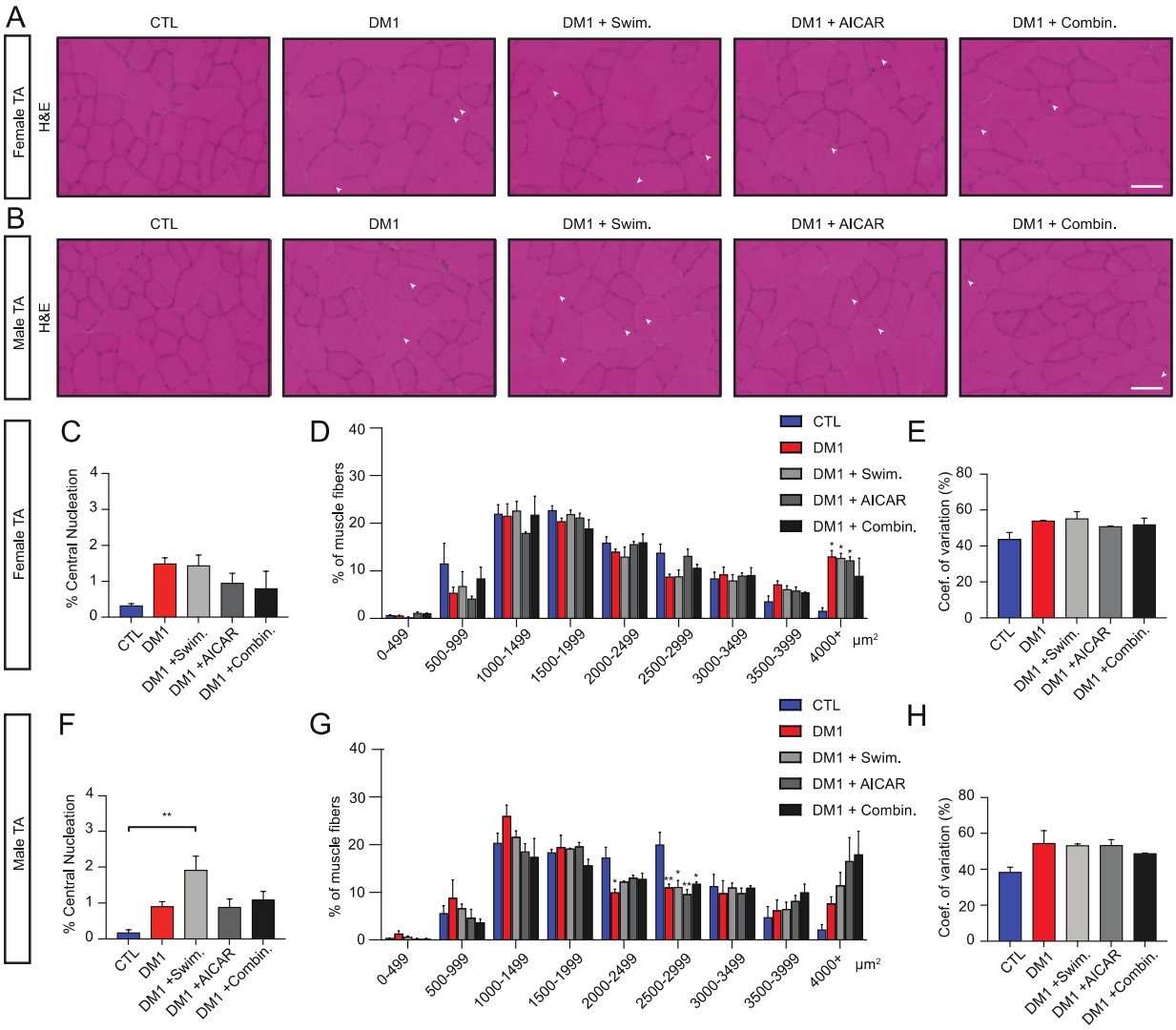

Figure 9. Impact of combinatorial treatment with exercise and AICAR on the histopathological characteristics of DM1 mouse TA muscles. (**A, B**) Representative H&E staining of TA muscles. Centrally located nuclei are indicated by arrows. (**C, F**) Percentages of central nucleation. (**D, G**) TA myofiber cross-sectional area. (**E, H**) Coefficient of variation of CSA. (**A, C, D, E**) Female TA muscles, N =3-4 and (**B, F, G, H**) Male TA muscles, N =3-4. One-way ANOVA was used followed by Tukey's post-hoc test (* $p < 0.05$, ** $p < 0.01$ vs. CTL). Scale bar = 50 µm.

We first analyzed changes in the prevalence of centrally located myonuclei, a key feature of the DM1 muscle histopathology. Indeed, central nucleation has been suggested to occur due to the incomplete maturation of skeletal muscle fibers in DM1 (76,147) and it can also be taken as a sign of muscle fiber degeneration/regeneration (2,148). As illustrated in **Figure 8,** the percentage of centrally located nuclei was significantly increased in EDL muscles of saline treated male ($p < 0.05$) and female ($p < 0.01$) DM1 mice compared to control mice (**Fig. 8C, F**). Swimming alone had no significant effect on the degree of central nucleation in female DM1 mice (**Fig. 8C**) but induced a 1.5-fold increase in male DM1 mice that failed to reach statistical significance ($p = 0.18$ vs. DM1) (**Fig. 8F**). Since centrally located nuclei are also indicative of skeletal muscle repair, this increase may have occurred in response to exercise-induced muscle damage (148). In comparison to saline treated DM1 mice, both AICAR and the combinatorial treatment showed a trend towards a decrease in the prevalence of central nucleation in both male and female DM1 mice by similar magnitudes (**Fig. 8C, F**). This trend was further observed in TA muscles of AICAR and combinatorially treated female DM1 mice, but not in male DM1 mice (**Fig. 9**).

In addition to central nucleation, we also assessed the distribution of muscle fiber size following four weeks of each treatment in male and female DM1 mice (**Fig. 8D, G**). We thus performed immunofluorescence (IF) staining on EDL cross-sections using an anti-laminin primary antibody (images not shown) to define the periphery of individual muscle fibers for cross-sectional area (CSA) analysis. In DM1 mice, the fiber size distribution has been previously shown to be shifted towards larger, hypertrophic muscle fibers (>3000 μm^2) in comparison to controls (51,79).

In line with this observation, our CSA analysis of the EDL muscle fibers from saline treated female DM1 mice demonstrated a modest shift in fiber size distribution towards larger fibers (>2000 μm^2) (**Fig. 8D**). Swimming exercise and AICAR treatment alone induced a mild shift in

the CSA frequency distribution towards the control phenotype (**Fig. 8D**). Interestingly, combinatorial treatment significantly increased the proportion of larger muscle fibers (between 2000 to 4000 μm^2) in female DM1 mice, relative to control ($p < 0.05$) and saline treated ($p < 0.05$) groups (**Fig. 6D**). In male mice, the CSA frequency distributions of saline treated, exercised, and AICAR-treated DM1 mice were not significantly altered as compared to the controls (**Fig. 8G**). In contrast to our findings with DM1 EDL muscles, the CSA frequency distributions of male and female DM1 TA muscles did not significantly differ between experimental groups (**Fig. 9**).

To examine changes in the variability of muscle fiber size which is higher in DM1 mice (79), we calculated the coefficient of variation (CV) in CSA for each experimental group (**Fig. 8E, H**). In comparison to control mice, the CV was significantly increased in saline treated female DM1 mice ($p < 0.001$) (**Fig. 8E**), but only mildly elevated in male DM1 mice ($p = 0.2$; **Fig. 8H**). For both sexes, we observed a trend in the normalization of the CV towards control levels in response to the combinatorial treatment which was more prominent in female DM1 mice ($p = 0.09$ vs. DM1) (**Fig. 8E, H**). Collectively, these data indicate that four weeks of combinatorial treatment elicit greater morphological benefits in EDL muscles of female DM1 mice as compared to males.

3.5 Both AICAR and the combinatorial treatment promote a shift towards a more oxidative phenotype in female DM1 mouse muscles.

Chronic AMPK activation is known to stimulate metabolic adaptations towards a more oxidative phenotype in skeletal muscle (112,114). To determine whether the 4-week combinatorial treatment enhanced this phenotypic shift in DM1 mouse muscles, we assessed changes in the protein expression levels of PGC-1α, a master regulator of mitochondrial biogenesis and downstream target of AMPK (115), as well as mitochondrial oxidative phosphorylation (OXPHOS) proteins CV-ATP5A, CII-SDHB, and CIV-MTCO1 (**Fig. 10**).

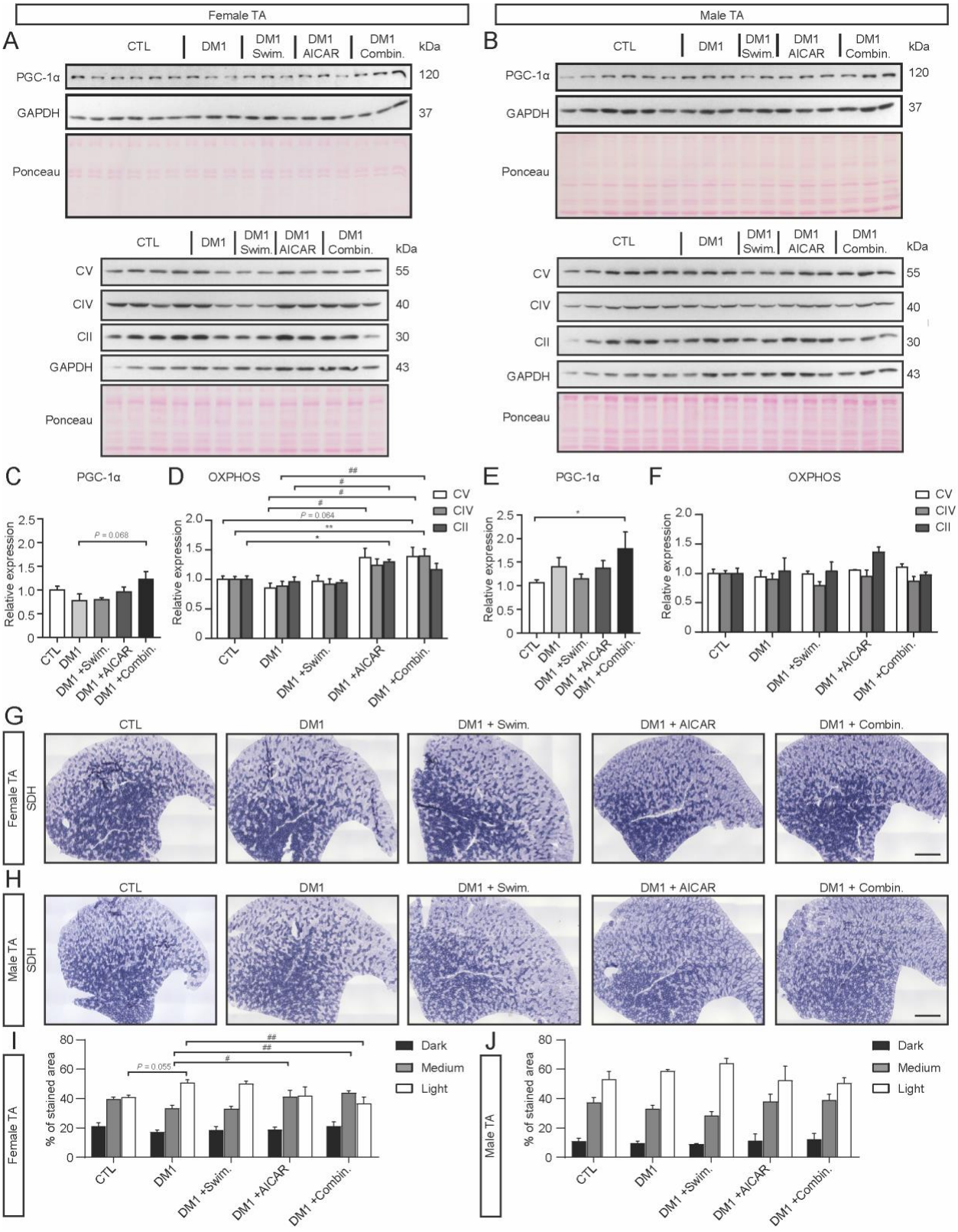
Female TA
Male TA
A
B
CTL
DM1
DM1 Swim.
DM1 AICAR
DM1 Combin.
kDa
PGC-1α
GAPDH
Ponceau
120
37
CV
CIV
CII
55
40
30
43
C
PGC-1α
D
OXPHOS
E
PGC-1α
F
OXPHOS
Relative expression
P = 0.068
P = 0.084
DM1 +Swim.
DM1 +AICAR
DM1 +Combin.
G
H
SDH
Female TA
Male TA
DM1 + Swim.
DM1 + AICAR
DM1 + Combin.
I
J
% of stained area
Dark
Medium
Light
P = 0.055

Figure 10. Treatment with AICAR individually and in combination with exercise promotes a more oxidative phenotype in female DM1 mouse muscles. (A, B) Representative Western blots of PGC-1α and OXPHOS proteins (CV-ATP5A, CIV-MTCO1 and CII-SDHB) in TA muscles. (**C, D, E, F**) Quantifications of protein expression levels normalized to Ponceau staining with mean +/- SEM. (**A, C, D**) Female TA muscles, N = 5-10 (**B, E, F**) Male TA muscles, N = 4-10. (G, H) Representative SDH staining (**I, J**) SDH-positive fiber distribution, N = 3-4. One-way ANOVA was used followed by Tukey's post-hoc test (* $p < 0.05$, ** $p < 0.01$ vs. CTL, # $p < 0.05$, ## $p < 0.01$ vs. DM1). Scale bar = 500 μm.

Our results show that PGC-1α protein expression levels trended towards an increase in the TA muscles of combinatorially treated female DM1 mice ($p = 0.068$ vs. DM1) and was only significantly elevated in comparison to control levels in male DM1 mice ($p < 0.05$) (**Fig. 10A-C, E**). The corresponding shift towards oxidative metabolism, as indicated by increased OXPHOS protein expression levels, was more prominent in AICAR- and combinatorially treated female DM1 mice (**Fig. 10A, D**) in comparison to males (**Fig. 10B, F**).

To complement these results, we also examined the relative oxidative capacity of DM1 muscles by performing succinate dehydrogenase staining on TA cross-sections (**Fig. 10G, H**). In comparison to saline treated DM1 mice, both AICAR and the combinatorial treatment significantly altered the distribution of SDH staining intensity towards a more oxidative phenotype in female DM1 mice (**Fig. 10G, I**), with no significant changes observed in male DM1 mice (**Fig. 10H, J**). To determine whether this shift towards enhanced oxidative metabolism in female DM1 mice was related to changes in muscle fiber type composition, we performed IF staining on TA cross-sections using anti-myosin heavy chain (MHC) type I-, IIA-, and IIB-specific primary antibodies (**Fig. 11**). We did not observe any significant alterations in fiber type ratios across all experimental groups in female DM1 TA muscles (**Fig. 11A, C**). A similar trend was observed in male TA muscles, which only displayed an increase in the percentage of oxidative type IIA muscle fibers ($p < 0.05$ vs. CTL) in the saline treated group, in comparison to control mice (**Fig. 11B, D**). Altogether, our results demonstrate that both AICAR and the combinatorial treatment induced a significant shift towards a more oxidative phenotype in muscles of female DM1 mice, without alterations in muscle fiber type composition.

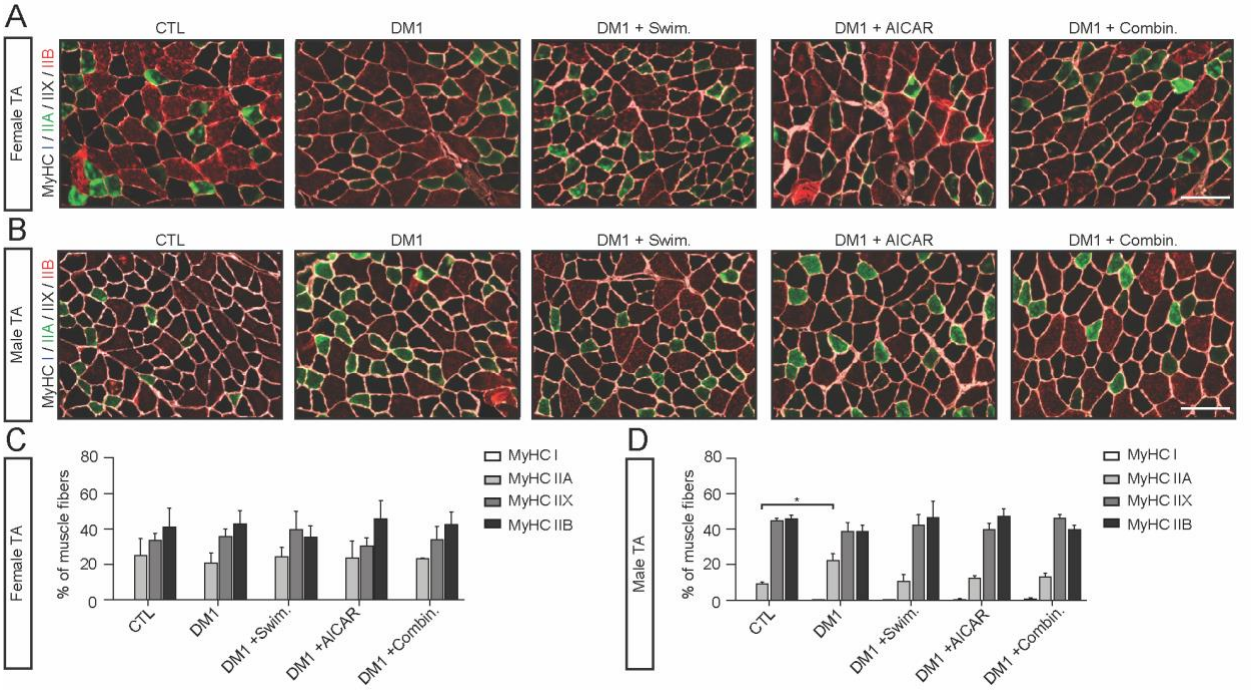

Figure 11. Combinatorial treatment with exercise and AICAR does not significantly alter muscle fiber type distribution in DM1 TA muscles. (**A, B**) Representative immunofluorescence images of MHC type I (blue), IIA (green), IIB (red) and Laminin (white). MHC type IIX remained unstained (black). (**C, D**) MHC-fiber type distribution. (**A, C**) Female TA muscles, N =3-4 and (**B, D**) Male TA muscles, N = 3-4. One-way ANOVA was used followed by Tukey's post-hoc test (* $p < 0.05$ vs. CTL). Scale bar = 100 μm.

Chapter 4: General Discussion

4.1 Summary

In the present study, we examined the effect of a 4-week combinatorial treatment strategy with swimming exercise and AICAR on the DM1 skeletal muscle phenotype in male and female DM1 mice. We demonstrate that this therapeutic approach improves the DM1 muscle phenotype and has a greater beneficial impact on female DM1 mouse muscles, in which the combinatorial treatment additively mitigated the nuclear accumulation of CUG^{exp} RNA foci and promoted muscle fiber hypertrophy. Our results further show a concomitant reduction in the sequestration of MBNL1 which was accompanied by the correction of key DM1 ASEs and reduced histopathological abnormalities in both AICAR- and combinatorially treated male and female DM1 mice. Our findings collectively reveal that exercise potentiates the beneficial impact of AICAR in mitigating the DM1 skeletal muscle pathology and that this combinatorial approach is particularly effective in female DM1 mice as compared to males.

4.1.1 AICAR and the combinatorial treatment elicit a more oxidative phenotype in female DM1 mouse muscle

Given that AICAR and exercise are potent stimulators of AMPK, an important question raised by our study is whether the beneficial effects of these combined interventions in DM1 skeletal muscle resulted from increased AMPK activation. Although the status of AMPK activation was not reported due to the time point at which tissue collection occurred, the shift towards a more oxidative skeletal muscle phenotype that is elicited by chronic AMPK stimulation (111,112,114) was observed in AICAR- and combinatorially treated female DM1 mice. This phenotypic shift was accompanied by a trend towards an increase in PGC1α protein abundance in the combinatorial treatment group only. Our results could suggest that the magnitude of AMPK

activation, as indicated by its chronic downstream effect on the level PGC1α protein, may have been greater in response to the combination of AICAR and exercise in female DM1 mice. In male DM1 mice, it remains unclear why the corresponding shift towards a more oxidative phenotype did not occur following the combinatorial treatment despite elevated PGC1α protein levels. Interestingly, we did not observe a significant reduction in PGC1α protein abundance that was previously reported and associated with reduced AMPK activation in our initial work (79). However, this result could have arisen from differences in the types of skeletal muscles (EDL vs. TA) and/or ages of DM1 mice (3-4 vs. 9-month-old) that were analyzed in these studies.

4.1.2 AICAR treatment and swimming exercise in combination promote muscle hypertrophy

In addition to mitigating key pathological features of DM1, an unexpected but potentially beneficial result of the combinatorial treatment was the skeletal muscle hypertrophy observed in female DM1 mice. Interestingly, the combination of AICAR treatment and exercise has been previously shown to promote muscle fiber hypertrophy in mouse models of chronic inflammatory myopathy (149) and DMD (150). Given that skeletal muscle weakness and wasting are prominent symptoms of DM1, this hypertrophic response could potentially prevent or delay the onset of these features in DM1 skeletal muscle.

While this finding also appears at first glance in contradiction with our initial reports of a more normalized muscle fiber CSA distribution following AICAR treatment (79), we hypothesize that improvements in the regulation of autophagy may underlie this hypertrophic response in DM1 mouse skeletal muscles. The dysregulation of autophagy has been suggested to promote skeletal muscle dysfunction due to the accumulation of damaged proteins and organelles (151). Multiple reports have suggested that pharmacological or physiological stimulation of autophagy is an

effective therapeutic approach to conserve skeletal muscle mass and function in several models of muscle degeneration (119,136,152–154). Since HSA^{LR} mouse muscles display impaired autophagy induction due to perturbed AMPK/mTORC1 signaling (75,78), the combination of AICAR and exercise may serve to upregulate autophagy, thereby enabling exercise-induced adaptations, including hypertrophy, to occur (155,156). In accordance with this potential mechanism, recent findings have suggested that exercise may beneficially stimulate autophagy in HSA^{LR} mouse skeletal muscles (129). It thus appears important to assess in future work the state of autophagy and associated signaling pathways in DM1 skeletal muscle in response to the combination of pharmacological and physiological AMPK activation.

4.1.3 Swimming exercise does not robustly improve the DM1 skeletal muscle phenotype

A parallel objective of our study was to determine whether swimming exercise would improve the DM1 skeletal muscle phenotype. In our initial work (79), Ravel-Chapuis *et al.* demonstrated that volitional wheel running exercise improved several MBNL1-dependent DM1 ASEs in HSA^{LR} mouse muscles. In line with these findings, subsequent studies have reported additional improvements in nuclear CUG^{exp} foci accumulation, aberrant alternative splicing, myotonia, and histological abnormalities following wheel and treadmill running exercise regimens (65,128). In contrast, results from the present study revealed a modest improvement in *Atp2a1* exon 22 missplicing in female DM1 mice only. The comparatively minimal effect of swimming is likely due to variations in the exercise parameters used (further discussed in section 5.2). Notably, the 4-week timeframe of our study was shorter in comparison to previous studies that have spanned 8-10 weeks (65,79,128), which might suggest a duration-dependent effect of exercise.

Interestingly, very recent reports that were published after the completion of our study have contradicted previous findings on the effect of exercise in DM1 skeletal muscle. Fifteen weeks of

moderate treadmill exercise were shown to partially improve DM1 ASEs and symptoms of fatigue in the absence of robust changes in nuclear CUG^{exp} RNA foci accumulation or MBNL1 sequestration in aged HSA^{LR} mouse gastrocnemius muscles (134). Findings from a recent clinical study have also demonstrated that a 12-week cycling program significantly improves the cardiorespiratory fitness and muscle function of DM1 patients without concomitant changes in RNA toxicity-related outcomes (130). Although these results imply that exercise-induced AMPK activation might not impact the fundamental characteristics of the DM1 skeletal muscle pathology, the functional improvements observed in HSA^{LR} mice and DM1 patients preserve the clinical relevance of exercise as a therapeutic intervention (130,134). Moreover, the present study highlights the potential advantage of its combination with pharmacological interventions that mitigate CUG^{exp} RNA toxicity.

4.1.4 The therapeutic potential of combinatorial interventions with exercise for DM1

In DM1 skeletal muscle, combinatorial therapeutic strategies have been previously shown to be effective in mitigating multiple disease features at both the molecular and functional level (66,134). To date, only one other study has evaluated the combination of exercise with other therapeutic interventions in the context of DM1 skeletal muscle. Hu *et al.* (134) previously demonstrated that combining antisense oligonucleotide treatment with moderate treadmill exercise attenuates the DM1 skeletal muscle pathology and fatigue in aged HSA^{LR} mice, while the individual application of each therapy improves one of these aspects but not the other. Our results suggest that the combination of AICAR treatment with exercise can potentiate the reduction of nuclear accumulation of CUG^{exp} foci and promote muscle fiber hypertrophy. However, the functional consequences of these improvements and those that may have been elicited by swimming exercise alone were not assessed in the present study and should be examined in future

work. The clinical translation of our findings is limited by the use of AICAR, which is not currently approved for administration in humans, as well as the feasibility of our exercise protocol in DM1 patients. However, this proof-of-concept work further establishes the potential of combining AMPK-based therapeutic approaches for DM1 which might be advantageous provided that several aspects, including the parameters of exercise (frequency, intensity, time, duration, and type), are optimized for application in patients.

4.2 Study Limitations

Although our exercise protocol accounted for important variables such as frequency, time, and type, one of the limitations of this study was the inability to quantify exercise intensity during swimming bouts due to the nature of the experimental set-up. Given that exercise-induced AMPK activation is intensity-dependent (157), this parameter remains an underlying factor that could have influenced the magnitude of disease correction as well as other phenotypic adaptations (e.g., fiber type switch) in DM1 mice. The use of an adjustable-flow swimming pool, as previously described (136,137), would permit the establishment of an absolute exercise intensity during swimming bouts and improve the reproducibility of our study. Moreover, the use of relative exercise intensity could ideally account for potential variations in exercise capacity between male and female DM1 mice (65); however, this measurement is not necessarily feasible with swimming exercise regimes. Future investigations that incorporate these elements would provide greater insight into the threshold of exercise intensity and, by consequence, magnitude of AMPK activation required for improvements in DM1 skeletal muscle to occur, while enabling a better comparison of treatment efficacy between experimental groups.

Another limitation of the present study arises from the lack of acute AMPK activation measurements in response to swimming exercise and AICAR treatment interventions alone or in

combination. The time point at which tissue harvesting occurred was intentionally chosen to assess chronic adaptations and would have precluded the detection of acute signaling changes elicited by exercise or AICAR in DM1 mouse skeletal muscles. Although our main objective was to examine the long-term impact of combining pharmacological and physiological AMPK activators on the DM1 skeletal muscle phenotype, our investigation would have benefited from time course experiments that validated acute skeletal muscle AMPK activation post-intervention. These experiments would reveal whether a greater magnitude or more prolonged stimulation of AMPK was elicited by the combinatorial treatment in comparison to AICAR or exercise alone, which could strengthen the conclusions of our study and provide a potential explanation for the differences observed between male and female DM1 mice and in different types of muscles. Given the important information that would be obtained from such work, future studies should evaluate the acute status of AMPK activation (as indicated by Thr172-phosphorylated AMPK relative to total AMPK protein abundance) and activity (as indicated by the level of phosphorylated ACC) in DM1 skeletal muscle in response to combinatorial treatments with AMPK agonists.

Lastly, one of the inherent limitations of the HSA^{LR} mouse model of DM1 is the absence of prominent skeletal muscle weakness and wasting symptoms. For this reason, we did not examine changes in skeletal muscle function in the present study, although these could have occurred in response to swimming exercise and AICAR treatment alone or in combination (149,150). Hu *et al*. (134) and Mikhail *et al*. (130) have previously shown that exercise therapy can elicit functional adaptations without improvements in the molecular phenotype in DM1 skeletal muscle, thereby highlighting the importance of evaluating such outcomes. Moreover, in light of our observations of muscle fiber hypertrophy following the combinatorial treatment, future studies should determine if functional benefits arise from this cellular response. Jones *et al*. (76)

previously suggested that grip strength is reduced in aged HSA^{LR} mice, which can also exhibit a progressive myopathy (134). Thus, it would be interesting to examine if the combination of pharmacological and physiological AMPK agonists could prevent or delay the onset of weakness in DM1 skeletal muscle by preserving muscle mass and/or integrity.

4.3 Future Directions

Several important questions raised by the findings and limitations of the present study warrant future investigation. Although our results further establish the therapeutic potential of AMPK-based interventions for DM1, the molecular mechanisms that underlie the beneficial impact of its activation on the DM1 skeletal muscle phenotype remain unknown. Moreover, our results do not exclude the potential therapeutic contribution(s) of AMPK-independent pathways that can be stimulated by AICAR or exercise in skeletal muscle (158,159). To date, the collection of evidence that implicates AMPK as an important molecular target in DM1 (described in section 1.4) has been obtained primarily through the use of indirect AMPK activators (75,79,126). Thus, mechanistic studies using gene knockout or direct pharmacological approaches, or a combination thereof, are needed to delineate the precise therapeutic role of AMPK in DM1. These investigations could take advantage of the recent emergence of direct pan-AMPK small molecule activators, such as MK-8722, that have been shown to allosterically activate AMPK by binding to the ADaM site (100,104). The specificity of these AMPK agonists would confirm the beneficial effects of its activation in DM1 skeletal muscle and provide greater insight into the degree to which previously reported improvements can be attributed to AMPK. Furthermore, complementary experiments using gene knockout models or AMPK inhibitors in combination with AICAR treatment could help elucidate the contributions of other cellular pathways whose modulation might be therapeutically relevant in DM1 skeletal muscle.

In addition to defining the molecular basis for AMPK-mediated improvements in DM1 skeletal muscle, future studies should also examine the impact of clinically relevant AMPK activators, such as O304 (105) or metformin (160), in combination with exercise interventions. As previously mentioned, the therapeutic application of AICAR in human beings has not received approval and is limited by its poor oral bioavailability, variable efficacy in clinical trials, and potential adverse effects at high doses (159,161). Similarly, the clinical translation of MK-8722 is prevented by its ability to promote cardiac hypertrophy (104), which remains a potential adverse effect of systemic AMPK activation that should be evaluated in the context of DM1. In contrast, O304 is a novel small molecular AMPK agonist has been shown to activate AMPK in skeletal muscle without inducing cardiac hypertrophy during systemic administration (105). Moreover, the therapeutic potential of O304 is further demonstrated by its oral bioavailability and previous use in a phase IIA clinical trial in type 2 diabetes patients (105). Metformin is another AMPK activator that is already FDA-approved and has been shown to improve mobility in DM1 patients (132). It is currently under evaluation in phase III clinical trials (131), and could therefore serve as an alternative pharmacological AMPK agonist in a combinatorial treatment with exercise for DM1. In light of recent findings from Nikolaidis *et al*. (162), which suggest that the bioavailability of metformin is increased with exercise in healthy individuals, we postulate that exercise could also potentiate disease correction in DM1 skeletal muscle by enhancing the bioavailability or systemic delivery of pharmacological AMPK activators. Although currently speculative, this hypothesis could be examined in future studies that account for the pharmacokinetic profiles of the aforementioned AMPK agonists in combination with exercise.

Lastly, the HSA^{LR} mouse model limits the scope of our investigation to DM1 skeletal muscle. To strengthen the clinical relevance of combinatorial DM1 treatments that target AMPK,

the impact of this therapeutic approach on other affected tissues in DM1 could possibly be evaluated using multisystemic preclinical models such as the DM200 mouse, which displays DM1-related impairments in both skeletal muscle and the heart (52). Such studies should include a comprehensive analysis of the systemic effects of activating AMPK in order to identify additional benefits and possible adverse effects (e.g., cardiac hypertrophy) that might arise from its chronic activation in other tissues.

4.4 Conclusion

DM1 is a highly complex neuromuscular disease for which there is no effective cure. In the present study, we examined the combined effect of the AMPK agonists, AICAR and exercise, on the DM1 skeletal muscle phenotype in HSA^{LR} mice. Our findings further establish the importance of targeting AMPK in DM1 and reveal that a combinatorial therapeutic approach with swimming exercise potentiates the effect of pharmacological AMPK activation, with a significant reduction in nuclear CUG^{exp} RNA foci accumulation observed in female DM1 mouse skeletal muscles. The combination of AICAR and exercise also promoted muscle fiber hypertrophy in female DM1 mice, which may protect against the onset of skeletal muscle weakness and wasting symptoms. In comparison to previous preclinical findings (65,79,128), swimming exercise alone did not markedly improve DM1 skeletal muscle features. As previously discussed, our results could be limited by variations in the intensity of exercise, which was unable to be quantified due to the nature of the exercise apparatus, as well as the contribution of AMPK-independent effects induced by AICAR or exercise. Future investigations that account for these parameters could increase the clinical relevance of this combinatorial treatment strategy and elucidate the mechanism(s) by which AMPK activation ameliorates the DM1 skeletal muscle pathology. Despite these limitations, the data presented in this thesis further associates the chronic activation

of AMPK with beneficial adaptations in DM1 skeletal muscle and highlights the therapeutic potential of combinatorial AMPK-based treatments for DM1.

References

1. Misquitta, N.S., Ravel-Chapuis, A. and Jasmin, B.J. (2023) Combinatorial treatment with exercise and AICAR potentiates the rescue of myotonic dystrophy type 1 mouse muscles in a sex-specific manner. *Hum. Mol. Genet.*, **32**, 551–566.
2. McNally, E.M. and Pytel, P. (2007) Muscle Diseases: The Muscular Dystrophies. *Annu. Rev. Pathol. Mech. Dis.*, **2**, 87–109.
3. Mathieu, J., Allard, P., Potvin, L., Prévost, C. and Bégin, P. (1999) A 10-year study of mortality in a cohort of patients with myotonic dystrophy. *Neurology*, **52**, 1658–1658.
4. Johnson, N.E., Butterfield, R.J., Mayne, K., Newcomb, T., Imburgia, C., Dunn, D., Duval, B., Feldkamp, M.L. and Weiss, R.B. (2021) Population-Based Prevalence of Myotonic Dystrophy Type 1 Using Genetic Analysis of Statewide Blood Screening Program. *Neurology*, **96**, e1045–e1053.
5. Liao, Q., Zhang, Y., He, J. and Huang, K. (2022) Global Prevalence of Myotonic Dystrophy: An Updated Systematic Review and Meta-Analysis. *Neuroepidemiology*, **56**, 163–173.
6. Mathieu, J. and Prévost, C. (2012) Epidemiological surveillance of myotonic dystrophy type 1: a 25-year population-based study. *Neuromuscul. Disord. NMD*, **22**, 974–979.
7. Yotova, V., Labuda, D., Zietkiewicz, E., Gehl, D., Lovell, A., Lefebvre, J.-F., Bourgeois, S., Lemieux-Blanchard, É., Labuda, M., Vézina, H., *et al.* (2005) Anatomy of a founder effect: myotonic dystrophy in Northeastern Quebec. *Hum. Genet.*, **117**, 177–187.
8. Thornton, C.A. (2014) Myotonic Dystrophy. *Neurol. Clin.*, **32**, 705–719.
9. Duda, J., Venkatesh, Y. and Groh, W. (2016) Causes and Predictors of Mortality in a Large U.S. Myotonic Dystrophy Type 1 Adult Cohort (P5.077). *Neurology*, **86**, P5.077.
10. Groh, W.J., Groh, M.R., Saha, C., Kincaid, J.C., Simmons, Z., Ciafaloni, E., Pourmand, R., Otten, R.F., Bhakta, D., Nair, G.V., *et al.* (2008) Electrocardiographic Abnormalities and Sudden Death in Myotonic Dystrophy Type 1. *N. Engl. J. Med.*, **358**, 2688–2697.
11. Turner, C. and Hilton-Jones, D. (2010) The myotonic dystrophies: diagnosis and management. *J. Neurol. Neurosurg. Psychiatry*, **81**, 358–367.
12. De Antonio, M., Dogan, C., Hamroun, D., Mati, M., Zerrouki, S., Eymard, B., Katsahian, S. and Bassez, G. (2016) Unravelling the myotonic dystrophy type 1 clinical spectrum: A systematic registry-based study with implications for disease classification. *Rev. Neurol. (Paris)*, **172**, 572–580.
13. de Die-Smulders, C.E., Höweler, C.J., Thijs, C., Mirandolle, J.F., Anten, H.B., Smeets, H.J., Chandler, K.E. and Geraedts, J.P. (1998) Age and causes of death in adult-onset myotonic dystrophy. *Brain*, **121**, 1557–1563.
14. Ashizawa, T., Gagnon, C., Groh, W.J., Gutmann, L., Johnson, N.E., Meola, G., Moxley, R., Pandya, S., Rogers, M.T., Simpson, E., *et al.* (2018) Consensus-based care recommendations for adults with myotonic dystrophy type 1. *Neurol. Clin. Pract.*, **8**, 507–520.
15. Landfeldt, E., Nikolenko, N., Jimenez-Moreno, C., Cumming, S., Monckton, D.G., Gorman, G., Turner, C. and Lochmüller, H. (2019) Disease burden of myotonic dystrophy type 1. *J. Neurol.*, **266**, 998–1006.
16. Brook, J.D., McCurrach, M.E., Harley, H.G., Buckler, A.J., Church, D., Aburatani, H., Hunter, K., Stanton, V.P., Thirion, J.-P., Hudson, T., *et al.* (1992) Molecular basis of

myotonic dystrophy: Expansion of a trinucleotide (CTG) repeat at the 3′ end of a transcript encoding a protein kinase family member. *Cell*, **68**, 799–808.
17. Mahadevan, M., Tsilfidis, C., Sabourin, L., Shutler, G., Amemiya, C., Jansen, G., Neville, C., Narang, M., Barceló, J., O'Hoy, K., *et al.* (1992) Myotonic Dystrophy Mutation: an Unstable CTG Repeat in the 3′ Untranslated region of the Gene. *Science*.
18. Seifert, B.A., Reddi, H.V., Kang, B.E., Bean, L.J.H., Shealy, A. and Rose, N.C. (2024) Myotonic dystrophy type 1 testing, 2024 revision: A technical standard of the American College of Medical Genetics and Genomics (ACMG). *Genet. Med.*, **0**.
19. Martorell, L., Monckton, D.G., Sanchez, A., Lopez de Munain, A. and Baiget, M. (2001) Frequency and stability of the myotonic dystrophy type 1 premutation. *Neurology*, **56**, 328–335.
20. Hunter, A., Tsilfidis, C., Mettler, G., Jacob, P., Mahadevan, M., Surh, L. and Korneluk, R. (1992) The correlation of age of onset with CTG trinucleotide repeat amplification in myotonic dystrophy. *J. Med. Genet.*, **29**, 774–779.
21. Overend, G., Légaré, C., Mathieu, J., Bouchard, L., Gagnon, C. and Monckton, D.G. (2019) Allele length of the DMPK CTG repeat is a predictor of progressive myotonic dystrophy type 1 phenotypes. *Hum. Mol. Genet.*, **28**, 2245–2254.
22. Muscular Dystrophy Association (2015) Causes/Inheritance - Myotonic Dystrophy (DM) - Diseases. Causes/Inheritance - Myotonic Dystrophy (DM) - Diseases https://www.mda.org/disease/myotonic-dystrophy/causes-inheritance (accessed Sep 4, 2024).
23. Fu, Y.-H., Friedman, D.L., Richards, S., Pearlman, J.A., Gibbs, R.A., Pizzuti, A., Ashizawa, T., Perryman, M.B., Scarlato, G., Raymond G. Fenwick, J., *et al.* (1993) Decreased expression of myotonin-protein kinase messenger RNA and protein in adult form of myotonic dystrophy. *Science*, **260**, 235–239.
24. Carrell, S.T., Carrell, E.M., Auerbach, D., Pandey, S.K., Bennett, C.F., Dirksen, R.T. and Thornton, C.A. (2016) Dmpk gene deletion or antisense knockdown does not compromise cardiac or skeletal muscle function in mice. *Hum. Mol. Genet.*, **25**, 4328–4338.
25. Jansen, G., Groenen, P.J.T.A., Bächner, D., Jap, P.H.K., Coerwinkel, M., Oerlemans, F., van den Broek, W., Gohlsch, B., Pette, D., Plomp, J.J., *et al.* (1996) Abnormal myotonic dystrophy protein kinase levels produce only mild myopathy in mice. *Nat. Genet.*, **13**, 316–324.
26. Reddy, S., Smith, D.B.J., Rich, M.M., Leferovich, J.M., Reilly, P., Davis, B.M., Tran, K., Rayburn, H., Bronson, R., Cros, D., *et al.* (1996) Mice lacking the myotonic dystrophy protein kinase develop a late onset progressive myopathy. *Nat. Genet.*, **13**, 325–335.
27. Klesert, T.R., Cho, D.H., Clark, J.I., Maylie, J., Adelman, J., Snider, L., Yuen, E.C., Soriano, P. and Tapscott, S.J. (2000) Mice deficient in Six5 develop cataracts: implications for myotonic dystrophy. *Nat. Genet.*, **25**, 105–109.
28. Taneja, K.L., McCurrach, M., Schalling, M., Housman, D. and Singer, R.H. (1995) Foci of trinucleotide repeat transcripts in nuclei of myotonic dystrophy cells and tissues. *J. Cell Biol.*, **128**, 995–1002.
29. Davis, B.M., McCurrach, M.E., Taneja, K.L., Singer, R.H. and Housman, D.E. (1997) Expansion of a CUG trinucleotide repeat in the 3′ untranslated region of myotonic

dystrophy protein kinase transcripts results in nuclear retention of transcripts. *Proc. Natl. Acad. Sci.*, **94**, 7388–7393.
30. Miller, J.W., Urbinati, C.R., Teng-umnuay, P., Stenberg, M.G., Byrne, B.J., Thornton, C.A. and Swanson, M.S. (2000) Recruitment of human muscleblind proteins to (CUG)n expansions associated with myotonic dystrophy. *EMBO J.*, **19**, 4439–4448.
31. Fardaei, M., Larkin, K., Brook, J.D. and Hamshere, M.G. (2001) In vivo co-localisation of MBNL protein with DMPK expanded-repeat transcripts. *Nucleic Acids Res.*, **29**, 2766–2771.
32. Mankodi, A., Urbinati, C.R., Yuan, Q.-P., Moxley, R.T., Sansone, V., Krym, M., Henderson, D., Schalling, M., Swanson, M.S. and Thornton, C.A. (2001) Muscleblind localizes to nuclear foci of aberrant RNA in myotonic dystrophy types 1 and 2. *Hum. Mol. Genet.*, **10**, 2165–2170.
33. Ho, T.H., Charlet-B, N., Poulos, M.G., Singh, G., Swanson, M.S. and Cooper, T.A. (2004) Muscleblind proteins regulate alternative splicing. *EMBO J.*, **23**, 3103–3112.
34. Lin, X., Miller, J.W., Mankodi, A., Kanadia, R.N., Yuan, Y., Moxley, R.T., Swanson, M.S. and Thornton, C.A. (2006) Failure of MBNL1-dependent post-natal splicing transitions in myotonic dystrophy. *Hum. Mol. Genet.*, **15**, 2087–2097.
35. Kanadia, R.N., Johnstone, K.A., Mankodi, A., Lungu, C., Thornton, C.A., Esson, D., Timmers, A.M., Hauswirth, W.W. and Swanson, M.S. (2003) A Muscleblind Knockout Model for Myotonic Dystrophy. *Science*, **302**, 1978–1980.
36. Kuyumcu-Martinez, N.M., Wang, G.-S. and Cooper, T.A. (2007) Increased steady state levels of CUGBP1 in Myotonic Dystrophy 1 are due to PKC-mediated hyper-phosphorylation. *Mol. Cell*, **28**, 68–78.
37. Wang, E.T., Ward, A.J., Cherone, J.M., Giudice, J., Wang, T.T., Treacy, D.J., Lambert, N.J., Freese, P., Saxena, T., Cooper, T.A., *et al.* (2015) Antagonistic regulation of mRNA expression and splicing by CELF and MBNL proteins. *Genome Res.*, **25**, 858–871.
38. Savkur, R.S., Philips, A.V. and Cooper, T.A. (2001) Aberrant regulation of insulin receptor alternative splicing is associated with insulin resistance in myotonic dystrophy. *Nat. Genet.*, **29**, 40–47.
39. Philips, A.V., Timchenko, L.T. and Cooper, T.A. (1998) Disruption of Splicing Regulated by a CUG-Binding Protein in Myotonic Dystrophy. *Science*.
40. Orengo, J.P., Chambon, P., Metzger, D., Mosier, D.R., Snipes, G.J. and Cooper, T.A. (2008) Expanded CTG repeats within the DMPK 3′ UTR causes severe skeletal muscle wasting in an inducible mouse model for myotonic dystrophy. *Proc. Natl. Acad. Sci. U. S. A.*, **105**, 2646–2651.
41. Li, M., Zhuang, Y., Batra, R., Thomas, J.D., Li, M., Nutter, C.A., Scotti, M.M., Carter, H.A., Wang, Z.J., Huang, X.-S., *et al.* (2020) HNRNPA1-induced spliceopathy in a transgenic mouse model of myotonic dystrophy. *Proc. Natl. Acad. Sci. U. S. A.*, **117**, 5472–5477.
42. Paul, S., Dansithong, W., Kim, D., Rossi, J., Webster, N.J.G., Comai, L. and Reddy, S. (2006) Interaction of muscleblind, CUG-BP1 and hnRNP H proteins in DM1-associated aberrant IR splicing. *EMBO J.*, **25**, 4271–4283.
43. Ravel-Chapuis, A., Bélanger, G., Yadava, R.S., Mahadevan, M.S., DesGroseillers, L., Côté, J. and Jasmin, B.J. (2012) The RNA-binding protein Staufen1 is increased in

DM1 skeletal muscle and promotes alternative pre-mRNA splicing. *J. Cell Biol.*, **196**, 699–712.
44. Kino, Y., Washizu, C., Oma, Y., Onishi, H., Nezu, Y., Sasagawa, N., Nukina, N. and Ishiura, S. (2009) MBNL and CELF proteins regulate alternative splicing of the skeletal muscle chloride channel CLCN1. *Nucleic Acids Res.*, **37**, 6477–6490.
45. Ward, A.J., Rimer, M., Killian, J.M., Dowling, J.J. and Cooper, T.A. (2010) CUGBP1 overexpression in mouse skeletal muscle reproduces features of myotonic dystrophy type 1. *Hum. Mol. Genet.*, **19**, 3614–3622.
46. Kanadia, R.N., Shin, J., Yuan, Y., Beattie, S.G., Wheeler, T.M., Thornton, C.A. and Swanson, M.S. (2006) Reversal of RNA missplicing and myotonia after muscleblind overexpression in a mouse poly(CUG) model for myotonic dystrophy. *Proc. Natl. Acad. Sci.*, **103**, 11748–11753.
47. Du, H., Cline, M.S., Osborne, R.J., Tuttle, D.L., Clark, T.A., Donohue, J.P., Hall, M.P., Shiue, L., Swanson, M.S., Thornton, C.A., *et al.* (2010) Aberrant alternative splicing and extracellular matrix gene expression in mouse models of myotonic dystrophy. *Nat. Struct. Mol. Biol.*, **17**, 187–193.
48. Lee, K.-Y., Li, M., Manchanda, M., Batra, R., Charizanis, K., Mohan, A., Warren, S.A., Chamberlain, C.M., Finn, D., Hong, H., *et al.* (2013) Compound loss of muscleblind-like function in myotonic dystrophy. *EMBO Mol. Med.*, **5**, 1887–1900.
49. Osborne, R.J., Lin, X., Welle, S., Sobczak, K., O'Rourke, J.R., Swanson, M.S. and Thornton, C.A. (2009) Transcriptional and post-transcriptional impact of toxic RNA in myotonic dystrophy. *Hum. Mol. Genet.*, **18**, 1471–1481.
50. Crawford Parks, T.E., Marcellus, K.A., Péladeau, C., Jasmin, B.J. and Ravel-Chapuis, A. (2020) Overexpression of Staufen1 in DM1 mouse skeletal muscle exacerbates dystrophic and atrophic features. *Hum. Mol. Genet.*, **29**, 2185–2199.
51. Mankodi, A., Logigian, E., Callahan, L., McClain, C., White, R., Henderson, D., Krym, M. and Thornton, C.A. (2000) Myotonic dystrophy in transgenic mice expressing an expanded CUG repeat. *Science*, **289**, 1769–1773.
52. Mahadevan, M.S., Yadava, R.S., Yu, Q., Balijepalli, S., Frenzel-McCardell, C.D., Bourne, T.D. and Phillips, L.H. (2006) Reversible model of RNA toxicity and cardiac conduction defects in myotonic dystrophy. *Nat. Genet.*, **38**, 1066–1070.
53. Seznec, H., Agbulut, O., Sergeant, N., Savouret, C., Ghestem, A., Tabti, N., Willer, J.-C., Ourth, L., Duros, C., Brisson, E., *et al.* (2001) Mice transgenic for the human myotonic dystrophy region with expanded CTG repeats display muscular and brain abnormalities. *Hum. Mol. Genet.*, **10**, 2717–2726.
54. Osborne, R.J. and Thornton, C.A. (2006) RNA-dominant diseases. *Hum. Mol. Genet.*, **15**, R162–R169.
55. Chau, A. and Kalsotra, A. (2015) Developmental insights into the pathology of and therapeutic strategies for DM1: Back to the basics. *Dev. Dyn.*, **244**, 377–390.
56. Nakamori, M., Sobczak, K., Puwanant, A., Welle, S., Eichinger, K., Pandya, S., Dekdebrun, J., Heatwole, C.R., McDermott, M.P., Chen, T., *et al.* (2013) Splicing biomarkers of disease severity in myotonic dystrophy. *Ann. Neurol.*, **74**, 862–872.
57. Wang, E.T., Treacy, D., Eichinger, K., Struck, A., Estabrook, J., Olafson, H., Wang, T.T., Bhatt, K., Westbrook, T., Sedehizadeh, S., *et al.* (2019) Transcriptome alterations in myotonic dystrophy skeletal muscle and heart. *Hum. Mol. Genet.*, **28**, 1312–1321.

58. Yamashita, Y., Matsuura, T., Shinmi, J., Amakusa, Y., Masuda, A., Ito, M., Kinoshita, M., Furuya, H., Abe, K., Ibi, T., *et al.* (2012) Four parameters increase the sensitivity and specificity of the exon array analysis and disclose 25 novel aberrantly spliced exons in myotonic dystrophy. *J. Hum. Genet.*, **57**, 368–374.
59. Mankodi, A., Takahashi, M.P., Jiang, H., Beck, C.L., Bowers, W.J., Moxley, R.T., Cannon, S.C. and Thornton, C.A. (2002) Expanded CUG Repeats Trigger Aberrant Splicing of ClC-1 Chloride Channel Pre-mRNA and Hyperexcitability of Skeletal Muscle in Myotonic Dystrophy. *Mol. Cell*, **10**, 35–44.
60. Charlet-B., N., Savkur, R.S., Singh, G., Philips, A.V., Grice, E.A. and Cooper, T.A. (2002) Loss of the Muscle-Specific Chloride Channel in Type 1 Myotonic Dystrophy Due to Misregulated Alternative Splicing. *Mol. Cell*, **10**, 45–53.
61. Jentsch, T.J., Stein, V., Weinreich, F. and Zdebik, A.A. (2002) Molecular Structure and Physiological Function of Chloride Channels. *Physiol. Rev.*, **82**, 503–568.
62. Lueck, J.D., Mankodi, A., Swanson, M.S., Thornton, C.A. and Dirksen, R.T. (2007) Muscle Chloride Channel Dysfunction in Two Mouse Models of Myotonic Dystrophy. *J. Gen. Physiol.*, **129**, 79–94.
63. Berg, J., Jiang, H., Thornton, C.A. and Cannon, S.C. (2004) Truncated ClC-1 mRNA in myotonic dystrophy exerts a dominant-negative effect on the Cl current. *Neurology*, **63**, 2371–2375.
64. Wheeler, T.M., Lueck, J.D., Swanson, M.S., Dirksen, R.T. and Thornton, C.A. (2007) Correction of ClC-1 splicing eliminates chloride channelopathy and myotonia in mouse models of myotonic dystrophy. *J. Clin. Invest.*, **117**, 3952–3957.
65. Manta, A., Stouth, D.W., Xhuti, D., Chi, L., Rebalka, I.A., Kalmar, J.M., Hawke, T.J. and Ljubicic, V. (2019) Chronic exercise mitigates disease mechanisms and improves muscle function in myotonic dystrophy type 1 mice. *J. Physiol.*, **597**, 1361–1381.
66. Jenquin, J.R., Yang, H., Huigens III, R.W., Nakamori, M. and Berglund, J.A. (2019) Combination Treatment of Erythromycin and Furamidine Provides Additive and Synergistic Rescue of Mis-splicing in Myotonic Dystrophy Type 1 Models. *ACS Pharmacol. Transl. Sci.*, **2**, 247–263.
67. Kimura, T., Nakamori, M., Lueck, J.D., Pouliquin, P., Aoike, F., Fujimura, H., Dirksen, R.T., Takahashi, M.P., Dulhunty, A.F. and Sakoda, S. (2005) Altered mRNA splicing of the skeletal muscle ryanodine receptor and sarcoplasmic/endoplasmic reticulum Ca2+-ATPase in myotonic dystrophy type 1. *Hum. Mol. Genet.*, **14**, 2189–2200.
68. Kimura, T., Lueck, J.D., Harvey, P.J., Pace, S.M., Ikemoto, N., Casarotto, M.G., Dirksen, R.T. and Dulhunty, A.F. (2009) Alternative splicing of RyR1 alters the efficacy of skeletal EC coupling. *Cell Calcium*, **45**, 264–274.
69. Fugier, C., Klein, A.F., Hammer, C., Vassilopoulos, S., Ivarsson, Y., Toussaint, A., Tosch, V., Vignaud, A., Ferry, A., Messaddeq, N., *et al.* (2011) Misregulated alternative splicing of BIN1 is associated with T tubule alterations and muscle weakness in myotonic dystrophy. *Nat. Med.*, **17**, 720–725.
70. Kuo, I.Y. and Ehrlich, B.E. (2015) Signaling in Muscle Contraction. *Cold Spring Harb. Perspect. Biol.*, **7**, a006023.
71. Gao, Z. and Cooper, T.A. (2013) Reexpression of pyruvate kinase M2 in type 1 myofibers correlates with altered glucose metabolism in myotonic dystrophy. *Proc. Natl. Acad. Sci. U. S. A.*, **110**, 13570–13575.

72. Tang, Z.Z., Yarotskyy, V., Wei, L., Sobczak, K., Nakamori, M., Eichinger, K., Moxley, R.T., Dirksen, R.T. and Thornton, C.A. (2012) Muscle weakness in myotonic dystrophy associated with misregulated splicing and altered gating of CaV1.1 calcium channel. *Hum. Mol. Genet.*, **21**, 1312–1324.
73. Yamashita, Y., Matsuura, T., Kurosaki, T., Amakusa, Y., Kinoshita, M., Ibi, T., Sahashi, K. and Ohno, K. (2014) LDB3 splicing abnormalities are specific to skeletal muscles of patients with myotonic dystrophy type 1 and alter its PKC binding affinity. *Neurobiol. Dis.*, **69**, 200–205.
74. Cisco, L.A., Sipple, M.T., Edwards, K.M., Thornton, C.A. and Lueck, J.D. Verapamil mitigates chloride and calcium bi-channelopathy in a myotonic dystrophy mouse model. *J. Clin. Invest.*, **134**, e173576.
75. Brockhoff, M., Rion, N., Chojnowska, K., Wiktorowicz, T., Eickhorst, C., Erne, B., Frank, S., Angelini, C., Furling, D., Rüegg, M.A., *et al.* (2017) Targeting deregulated AMPK/mTORC1 pathways improves muscle function in myotonic dystrophy type I. *J. Clin. Invest.*, **127**, 549–563.
76. Jones, K., Wei, C., Iakova, P., Bugiardini, E., Schneider-Gold, C., Meola, G., Woodgett, J., Killian, J., Timchenko, N.A. and Timchenko, L.T. (2012) GSK3β mediates muscle pathology in myotonic dystrophy. *J. Clin. Invest.*, **122**, 4461–4472.
77. Yadava, R.S., Foff, E.P., Yu, Q., Gladman, J.T., Kim, Y.K., Bhatt, K.S., Thornton, C.A., Zheng, T.S. and Mahadevan, M.S. (2015) TWEAK/Fn14, a pathway and novel therapeutic target in myotonic dystrophy. *Hum. Mol. Genet.*, **24**, 2035–2048.
78. Leduc-Gaudet, J.-P., Franco-Romero, A., Cefis, M., Moamer, A., Broering, F.E., Milan, G., Sartori, R., Chaffer, T.J., Dulac, M., Marcangeli, V., *et al.* (2023) MYTHO is a novel regulator of skeletal muscle autophagy and integrity. *Nat. Commun.*, **14**, 1199.
79. Ravel-Chapuis, A., Al-Rewashdy, A., Bélanger, G. and Jasmin, B.J. (2018) Pharmacological and physiological activation of AMPK improves the spliceopathy in DM1 mouse muscles. *Hum. Mol. Genet.*, **27**, 3361–3376.
80. Wang, M., Weng, W.-C., Stock, L., Lindquist, D., Martinez, A., Gourdon, G., Timchenko, N., Snape, M. and Timchenko, L. (2019) Correction of Glycogen Synthase Kinase 3 *β* in Myotonic Dystrophy 1 Reduces the Mutant RNA and Improves Postnatal Survival of DMSXL Mice. *Mol. Cell. Biol.*, **39**, e00155-19.
81. Ravel-Chapuis, A., Bélanger, G., Côté, J., Michel, R.N. and Jasmin, B.J. (2017) Misregulation of calcium-handling proteins promotes hyperactivation of calcineurin-NFAT signaling in skeletal muscle of DM1 mice. *Hum. Mol. Genet.*, **26**, 2192–2206.
82. Da Poian, A.T., El-Bacha, T. and Luz, M.R.M. (2010) Nutrient Utilization in Humans: Metabolism Pathways. *Nat. Educ.*, **3**, 11.
83. Kemp, B.E., Mitchelhill, K.I., Stapleton, D., Michell, B.J., Chen, Z.-P. and Witters, L.A. (1999) Dealing with energy demand: the AMP-activated protein kinase. *Trends Biochem. Sci.*, **24**, 22–25.
84. Woods, A., Cheung, P.C.F., Smith, F.C., Davison, M.D., Scott, J., Beri, R.K. and Carling, D. (1996) Characterization of AMP-activated Protein Kinase β and γ Subunits: Assembly of the Heterotrimeric Complex In Vitro. *J. Biol. Chem.*, **271**, 10282–10290.
85. Cheung, P.C.F., Salt, I.P., Davies, S.P., Hardie, D.G. and Carling, D. (2000) Characterization of AMP-activated protein kinase γ-subunit isoforms and their role in AMP binding. *Biochem. J.*, **346**, 659–669.

86. Sanders, M.J., Grondin, P.O., Hegarty, B.D., Snowden, M.A. and Carling, D. (2007) Investigating the mechanism for AMP activation of the AMP-activated protein kinase cascade. *Biochem. J.*, **403**, 139–148.
87. Oakhill, J.S., Chen, Z.-P., Scott, J.W., Steel, R., Castelli, L.A., Ling, N., Macaulay, S.L. and Kemp, B.E. (2010) β-Subunit myristoylation is the gatekeeper for initiating metabolic stress sensing by AMP-activated protein kinase (AMPK). *Proc. Natl. Acad. Sci.*, **107**, 19237–19241.
88. Stapleton, D., Mitchelhill, K.I., Gao, G., Widmer, J., Michell, B.J., Teh, T., House, C.M., Fernandez, C.S., Cox, T., Witters, L.A., *et al.* (1996) Mammalian AMP-activated Protein Kinase Subfamily (∗). *J. Biol. Chem.*, **271**, 611–614.
89. Wu, J., Puppala, D., Feng, X., Monetti, M., Lapworth, A.L. and Geoghegan, K.F. (2013) Chemoproteomic Analysis of Intertissue and Interspecies Isoform Diversity of AMP-activated Protein Kinase (AMPK). *J. Biol. Chem.*, **288**, 35904–35912.
90. Salt, I.P., Johnson, G., Ashcroft, S.J.H. and Hardie, D.G. (1998) AMP-activated protein kinase is activated by low glucose in cell lines derived from pancreatic β cells, and may regulate insulin release. *Biochem. J.*, **335**, 533–539.
91. Winder, W.W. and Hardie, D.G. (1996) Inactivation of acetyl-CoA carboxylase and activation of AMP-activated protein kinase in muscle during exercise. *Am. J. Physiol.-Endocrinol. Metab.*, **270**, E299–E304.
92. Gowans, G.J. and Hardie, D.G. (2014) AMPK – a cellular energy sensor primarily regulated by AMP. *Biochem. Soc. Trans.*, **42**, 71–75.
93. Woods, A., Johnstone, S.R., Dickerson, K., Leiper, F.C., Fryer, L.G.D., Neumann, D., Schlattner, U., Wallimann, T., Carlson, M. and Carling, D. (2003) LKB1 Is the Upstream Kinase in the AMP-Activated Protein Kinase Cascade. *Curr. Biol.*, **13**, 2004–2008.
94. Hawley, S.A., Boudeau, J., Reid, J.L., Mustard, K.J., Udd, L., Mäkelä, T.P., Alessi, D.R. and Hardie, D.G. (2003) Complexes between the LKB1 tumor suppressor, STRADα/β and MO25α/β are upstream kinases in the AMP-activated protein kinase cascade. *J. Biol.*, **2**, 28.
95. Davies, S.P., Helps, N.R., Cohen, P.T. and Hardie, D.G. (1995) 5'-AMP inhibits dephosphorylation, as well as promoting phosphorylation, of the AMP-activated protein kinase. Studies using bacterially expressed human protein phosphatase-2C alpha and native bovine protein phosphatase-2AC. *FEBS Lett.*, **377**, 421–425.
96. Gowans, G.J., Hawley, S.A., Ross, F.A. and Hardie, D.G. (2013) AMP Is a True Physiological Regulator of AMP-Activated Protein Kinase by Both Allosteric Activation and Enhancing Net Phosphorylation. *Cell Metab.*, **18**, 556–566.
97. Willows, R., Sanders, M.J., Xiao, B., Patel, B.R., Martin, S.R., Read, J., Wilson, J.R., Hubbard, J., Gamblin, S.J. and Carling, D. (2017) Phosphorylation of AMPK by upstream kinases is required for activity in mammalian cells. *Biochem. J.*, **474**, 3059–3073.
98. Suter, M., Riek, U., Tuerk, R., Schlattner, U., Wallimann, T. and Neumann, D. (2006) Dissecting the Role of 5′-AMP for Allosteric Stimulation, Activation, and Deactivation of AMP-activated Protein Kinase *. *J. Biol. Chem.*, **281**, 32207–32216.
99. Woods, A., Dickerson, K., Heath, R., Hong, S.-P., Momcilovic, M., Johnstone, S.R., Carlson, M. and Carling, D. (2005) Ca2+/calmodulin-dependent protein kinase kinase-

beta acts upstream of AMP-activated protein kinase in mammalian cells. *Cell Metab.*, **2**, 21–33.

100. Cokorinos, E.C., Delmore, J., Reyes, A.R., Albuquerque, B., Kjøbsted, R., Jørgensen, N.O., Tran, J.-L., Jatkar, A., Cialdea, K., Esquejo, R.M., *et al.* (2017) Activation of Skeletal Muscle AMPK Promotes Glucose Disposal and Glucose Lowering in Non-human Primates and Mice. *Cell Metab.*, **25**, 1147-1159.e10.
101. Sullivan, J.E., Brocklehurst, K.J., Marley, A.E., Carey, F., Carling, D. and Beri, R.K. (1994) Inhibition of lipolysis and lipogenesis in isolated rat adipocytes with AICAR, a cell-permeable activator of AMP-activated protein kinase. *FEBS Lett.*, **353**, 33–36.
102. Corton, J.M., Gillespie, J.G., Hawley, S.A. and Hardie, D.G. (1995) 5-Aminoimidazole-4-Carboxamide Ribonucleoside. *Eur. J. Biochem.*, **229**, 558–565.
103. Zhou, G., Myers, R., Li, Y., Chen, Y., Shen, X., Fenyk-Melody, J., Wu, M., Ventre, J., Doebber, T., Fujii, N., *et al.* (2001) Role of AMP-activated protein kinase in mechanism of metformin action. *J. Clin. Invest.*, **108**, 1167–1174.
104. Myers, R.W., Guan, H.-P., Ehrhart, J., Petrov, A., Prahalada, S., Tozzo, E., Yang, X., Kurtz, M.M., Trujillo, M., Trotter, D.G., *et al.* (2017) Systemic pan-AMPK activator MK-8722 improves glucose homeostasis but induces cardiac hypertrophy. *Science*.
105. Steneberg, P., Lindahl, E., Dahl, U., Lidh, E., Straseviciene, J., Backlund, F., Kjellkvist, E., Berggren, E., Lundberg, I., Bergqvist, I., *et al.* PAN-AMPK activator O304 improves glucose homeostasis and microvascular perfusion in mice and type 2 diabetes patients. *JCI Insight*, **3**, e99114.
106. Owen, M.R., Doran, E. and Halestrap, A.P. (2000) Evidence that metformin exerts its anti-diabetic effects through inhibition of complex 1 of the mitochondrial respiratory chain. *Biochem. J.*, **348**, 607–614.
107. Stephenne, X., Foretz, M., Taleux, N., Zon, G.C. van der, Sokal, E., Hue, L., Viollet, B. and Guigas, B. (2011) Metformin activates AMP-activated protein kinase in primary human hepatocytes by decreasing cellular energy status. *Diabetologia*, **54**, 3101.
108. Xiao, B., Sanders, M.J., Carmena, D., Bright, N.J., Haire, L.F., Underwood, E., Patel, B.R., Heath, R.B., Walker, P.A., Hallen, S., *et al.* (2013) Structural basis of AMPK regulation by small molecule activators. *Nat. Commun.*, **4**, 3017.
109. Steinberg, G.R. and Hardie, D.G. (2023) New insights into activation and function of the AMPK. *Nat. Rev. Mol. Cell Biol.*, **24**, 255–272.
110. Kjøbsted, R., Hingst, J.R., Fentz, J., Foretz, M., Sanz, M.-N., Pehmøller, C., Shum, M., Marette, A., Mounier, R., Treebak, J.T., *et al.* (2018) AMPK in skeletal muscle function and metabolism. *FASEB J.*, **32**, 1741–1777.
111. Winder, W.W., Holmes, B.F., Rubink, D.S., Jensen, E.B., Chen, M. and Holloszy, J.O. (2000) Activation of AMP-activated protein kinase increases mitochondrial enzymes in skeletal muscle. *J. Appl. Physiol.*, **88**, 2219–2226.
112. Suwa, M., Nakano, H. and Kumagai, S. (2003) Effects of chronic AICAR treatment on fiber composition, enzyme activity, UCP3, and PGC-1 in rat muscles. *J. Appl. Physiol.*, **95**, 960–968.
113. Röckl, K.S.C., Hirshman, M.F., Brandauer, J., Fujii, N., Witters, L.A. and Goodyear, L.J. (2007) Skeletal Muscle Adaptation to Exercise Training : AMP-Activated Protein Kinase Mediates Muscle Fiber Type Shift. *Diabetes*, **56**, 2062–2069.

114. Narkar, V.A., Downes, M., Yu, R.T., Embler, E., Wang, Y.-X., Banayo, E., Mihaylova, M.M., Nelson, M.C., Zou, Y., Juguilon, H., *et al.* (2008) AMPK and PPARδ Agonists Are Exercise Mimetics. *Cell*, **134**, 405–415.
115. Jäger, S., Handschin, C., St-Pierre, J. and Spiegelman, B.M. (2007) AMP-activated protein kinase (AMPK) action in skeletal muscle via direct phosphorylation of PGC-1alpha. *Proc. Natl. Acad. Sci. U. S. A.*, **104**, 12017–12022.
116. Thomson, D.M. (2018) The Role of AMPK in the Regulation of Skeletal Muscle Size, Hypertrophy, and Regeneration. *Int. J. Mol. Sci.*, **19**, 3125.
117. Bolster, D.R., Crozier, S.J., Kimball, S.R. and Jefferson, L.S. (2002) AMP-activated Protein Kinase Suppresses Protein Synthesis in Rat Skeletal Muscle through Down-regulated Mammalian Target of Rapamycin (mTOR) Signaling *. *J. Biol. Chem.*, **277**, 23977–23980.
118. Sanchez, A.M.J., Csibi, A., Raibon, A., Cornille, K., Gay, S., Bernardi, H. and Candau, R. (2012) AMPK promotes skeletal muscle autophagy through activation of forkhead FoxO3a and interaction with Ulk1. *J. Cell. Biochem.*, **113**, 695–710.
119. Wright, N.A., Wilcox, S.H. and Thomson, D.M. (2019) Month-long AICAR Treatment Reverses Age-related mTOR Pathway Hyperactivity. *FASEB J.*, **33**, 539.9-539.9.
120. Masiero, E., Agatea, L., Mammucari, C., Blaauw, B., Loro, E., Komatsu, M., Metzger, D., Reggiani, C., Schiaffino, S. and Sandri, M. (2009) Autophagy Is Required to Maintain Muscle Mass. *Cell Metab.*, **10**, 507–515.
121. Dial, A.G., Ng, S.Y., Manta, A. and Ljubicic, V. (2018) The Role of AMPK in Neuromuscular Biology and Disease. *Trends Endocrinol. Metab.*, **29**, 300–312.
122. Ljubicic, V., Miura, P., Burt, M., Boudreault, L., Khogali, S., Lunde, J.A., Renaud, J.-M. and Jasmin, B.J. (2011) Chronic AMPK activation evokes the slow, oxidative myogenic program and triggers beneficial adaptations in mdx mouse skeletal muscle. *Hum. Mol. Genet.*, **20**, 3478–3493.
123. Ljubicic, V., Burt, M., Lunde, J.A. and Jasmin, B.J. (2014) Resveratrol induces expression of the slow, oxidative phenotype in mdx mouse muscle together with enhanced activity of the SIRT1-PGC-1α axis. *Am. J. Physiol. Cell Physiol.*, **307**, C66-82.
124. Ljubicic, V., Khogali, S., Renaud, J.-M. and Jasmin, B.J. (2012) Chronic AMPK stimulation attenuates adaptive signaling in dystrophic skeletal muscle. *Am. J. Physiol.-Cell Physiol.*, **302**, C110–C121.
125. Al-Rewashdy, H., Ljubicic, V., Lin, W., Renaud, J.-M. and Jasmin, B.J. (2015) Utrophin A is essential in mediating the functional adaptations of mdx mouse muscle following chronic AMPK activation. *Hum. Mol. Genet.*, **24**, 1243–1255.
126. Laustriat, D., Gide, J., Barrault, L., Chautard, E., Benoit, C., Auboeuf, D., Boland, A., Battail, C., Artiguenave, F., Deleuze, J.-F., *et al.* (2015) In Vitro and In Vivo Modulation of Alternative Splicing by the Biguanide Metformin. *Mol. Ther. Nucleic Acids*, **4**, e262.
127. González, A., Hall, M.N., Lin, S.-C. and Hardie, D.G. (2020) AMPK and TOR: The Yin and Yang of Cellular Nutrient Sensing and Growth Control. *Cell Metab.*, **31**, 472–492.
128. Sharp, L., Cox, D.C. and Cooper, T.A. (2019) Endurance exercise leads to beneficial molecular and physiological effects in a mouse model of myotonic dystrophy type 1. *Muscle Nerve*, **60**, 779–789.

129. Mikhail, A.I., Manta, A., Ng, S.Y., Osborne, A.K., Mattina, S.R., Mackie, M.R. and Ljubicic, V. (2023) A single dose of exercise stimulates skeletal muscle mitochondrial plasticity in myotonic dystrophy type 1. *Acta Physiol.*, **237**, e13943.
130. Mikhail, A.I., Nagy, P.L., Manta, K., Rouse, N., Manta, A., Ng, S.Y., Nagy, M.F., Smith, P., Lu, J.-Q., Nederveen, J.P., *et al.* (2022) Aerobic exercise elicits clinical adaptations in myotonic dystrophy type 1 patients independently of pathophysiological changes. *J. Clin. Invest.*, **132**, e156125.
131. Pascual-Gilabert, M., Artero, R. and López-Castel, A. (2023) The myotonic dystrophy type 1 drug development pipeline: 2022 edition. *Drug Discov. Today*, **28**, 103489.
132. Bassez, G., Audureau, E., Hogrel, J.-Y., Arrouasse, R., Baghdoyan, S., Bhugaloo, H., Gourlay-Chu, M.-L., Le Corvoisier, P. and Peschanski, M. (2018) Improved mobility with metformin in patients with myotonic dystrophy type 1: a randomized controlled trial. *Brain*, **141**, 2855–2865.
133. Roussel, M.-P., Morin, M., Gagnon, C. and Duchesne, E. (2019) What is known about the effects of exercise or training to reduce skeletal muscle impairments of patients with myotonic dystrophy type 1? A scoping review. *BMC Musculoskelet. Disord.*, **20**, 101.
134. Hu, N., Kim, E., Antoury, L., Li, J., González-Pérez, P., Rutkove, S.B. and Wheeler, T.M. (2021) Antisense oligonucleotide and adjuvant exercise therapy reverse fatigue in old mice with myotonic dystrophy. *Mol. Ther. - Nucleic Acids*, **23**, 393–405.
135. Ravel-Chapuis, A. and Jasmin, B.J. (2022) Combinatorial therapies for rescuing myotonic dystrophy type 1 skeletal muscle defects. *Trends Mol. Med.*, **28**, 439–442.
136. Desseille, C., Deforges, S., Biondi, O., Houdebine, L., D'amico, D., Lamazière, A., Caradeuc, C., Bertho, G., Bruneteau, G., Weill, L., *et al.* (2017) Specific Physical Exercise Improves Energetic Metabolism in the Skeletal Muscle of Amyotrophic-Lateral- Sclerosis Mice. *Front. Mol. Neurosci.*, **10**, 332.
137. Houdebine, L., D'Amico, D., Bastin, J., Chali, F., Desseille, C., Rumeau, V., Soukkari, J., Oudot, C., Rouquet, T., Bariohay, B., *et al.* (2019) Low-Intensity Running and High-Intensity Swimming Exercises Differentially Improve Energy Metabolism in Mice With Mild Spinal Muscular Atrophy. *Front. Physiol.*, **10**, 1258.
138. Roy, R.R., Hirota, W.K., Kuehl, M. and Edgerton, R. (1985) Recruitment patterns in the rat hindlimb muscle during swimming. *Brain Res.*, **337**, 175–178.
139. Roy, R.R., Hutchison, D.L., Pierotti, D.J., Hodgson, J.A. and Edgerton, V.R. (1991) EMG patterns of rat ankle extensors and flexors during treadmill locomotion and swimming. *J. Appl. Physiol. Bethesda Md 1985*, **70**, 2522–2529.
140. Corbett, M.A., Robinson, C.S., Dunglison, G.F., Yang, N., Joya, J.E., Stewart, A.W., Schnell, C., Gunning, P.W., North, K.N. and Hardeman, E.C. (2001) A mutation in α-tropomyosinslow affects muscle strength, maturation and hypertrophy in a mouse model for nemaline myopathy. *Hum. Mol. Genet.*, **10**, 317–328.
141. Tinsley, J.M., Potter, A.C., Phelps, S.R., Fisher, R., Trickett, J.I. and Davies, K.E. (1996) Amelioration of the dystrophic phenotype of mdx mice using a truncated utrophin transgene. *Nature*, **384**, 349–353.
142. Dogan, C., Antonio, M.D., Hamroun, D., Varet, H., Fabbro, M., Rougier, F., Amarof, K., Bes, M.-C.A., Bedat-Millet, A.-L., Behin, A., *et al.* (2016) Gender as a Modifying Factor Influencing Myotonic Dystrophy Type 1 Phenotype Severity and Mortality: A Nationwide Multiple Databases Cross-Sectional Observational Study. *PLOS ONE*, **11**, e0148264.

143. Raymond, K., Levasseur, M., Mathieu, J., Desrosiers, J. and Gagnon, C. (2017) A 9-year follow-up study of the natural progression of upper limb performance in myotonic dystrophy type 1: A similar decline for phenotypes but not for gender. *Neuromuscul. Disord.*, **27**, 673–682.
144. Evangelista, F.S., Brum, P.C. and Krieger, J.E. (2003) Duration-controlled swimming exercise training induces cardiac hypertrophy in mice. *Braz. J. Med. Biol. Res. Rev. Bras. Pesqui. Medicas E Biol.*, **36**, 1751–1759.
145. Stringer, C., Wang, T., Michaelos, M. and Pachitariu, M. (2021) Cellpose: a generalist algorithm for cellular segmentation. *Nat. Methods*, **18**, 100–106.
146. Waisman, A., Norris, A.M., Elías Costa, M. and Kopinke, D. (2021) Automatic and unbiased segmentation and quantification of myofibers in skeletal muscle. *Sci. Rep.*, **11**, 11793.
147. Pisani, V., Panico, M.B., Terracciano, C., Bonifazi, E., Meola, G., Novelli, G., Bernardi, G., Angelini, C. and Massa, R. (2008) Preferential central nucleation of type 2 myofibers is an invariable feature of myotonic dystrophy type 2. *Muscle Nerve*, **38**, 1405–1411.
148. Chargé, S.B.P. and Rudnicki, M.A. (2004) Cellular and molecular regulation of muscle regeneration. *Physiol. Rev.*, **84**, 209–238.
149. Saito, Y., Chikenji, T.S., Matsumura, T., Nakano, M. and Fujimiya, M. (2020) Exercise enhances skeletal muscle regeneration by promoting senescence in fibro-adipogenic progenitors. *Nat. Commun.*, **11**, 889.
150. Júnior, C.R.B., Pantaleão, L.C., Voltarelli, V.A., Bozi, L.H.M., Brum, P.C. and Zatz, M. (2012) Combined Effect of AMPK/PPAR Agonists and Exercise Training in mdx Mice Functional Performance. *PLOS ONE*, **7**, e45699.
151. Sandri, M., Coletto, L., Grumati, P. and Bonaldo, P. (2013) Misregulation of autophagy and protein degradation systems in myopathies and muscular dystrophies. *J. Cell Sci.*, **126**, 5325–5333.
152. Bujak, A.L., Crane, J.D., Lally, J.S., Ford, R.J., Kang, S.J., Rebalka, I.A., Green, A.E., Kemp, B.E., Hawke, T.J., Schertzer, J.D., *et al.* (2015) AMPK Activation of Muscle Autophagy Prevents Fasting-Induced Hypoglycemia and Myopathy during Aging. *Cell Metab.*, **21**, 883–890.
153. Campos, J.C., Baehr, L.M., Gomes, K.M.S., Bechara, L.R.G., Voltarelli, V.A., Bozi, L.H.M., Ribeiro, M.A.C., Ferreira, N.D., Moreira, J.B.N., Brum, P.C., *et al.* (2018) Exercise prevents impaired autophagy and proteostasis in a model of neurogenic myopathy. *Sci. Rep.*, **8**, 11818.
154. Pauly, M., Daussin, F., Burelle, Y., Li, T., Godin, R., Fauconnier, J., Koechlin-Ramonatxo, C., Hugon, G., Lacampagne, A., Coisy-Quivy, M., *et al.* (2012) AMPK activation stimulates autophagy and ameliorates muscular dystrophy in the mdx mouse diaphragm. *Am. J. Pathol.*, **181**, 583–592.
155. Lira, V.A., Okutsu, M., Zhang, M., Greene, N.P., Laker, R.C., Breen, D.S., Hoehn, K.L. and Yan, Z. (2013) Autophagy is required for exercise training-induced skeletal muscle adaptation and improvement of physical performance. *FASEB J.*, **27**, 4184–4193.
156. Sanchez, A.M.J., Bernardi, H., Py, G. and Candau, R.B. (2014) Autophagy is essential to support skeletal muscle plasticity in response to endurance exercise. *Am. J. Physiol.-Regul. Integr. Comp. Physiol.*, **307**, R956–R969.

157. Wojtaszewski, J.F., Nielsen, P., Hansen, B.F., Richter, E.A. and Kiens, B. (2000) Isoform-specific and exercise intensity-dependent activation of 5'-AMP-activated protein kinase in human skeletal muscle. *J. Physiol.*, **528 Pt 1**, 221–226.
158. Hoffman, N.J., Parker, B.L., Chaudhuri, R., Fisher-Wellman, K.H., Kleinert, M., Humphrey, S.J., Yang, P., Holliday, M., Trefely, S., Fazakerley, D.J., *et al.* (2015) Global Phosphoproteomic Analysis of Human Skeletal Muscle Reveals a Network of Exercise-Regulated Kinases and AMPK Substrates. *Cell Metab.*, **22**, 922–935.
159. Višnjić, D., Lalić, H., Dembitz, V., Tomić, B. and Smoljo, T. (2021) AICAr, a Widely Used AMPK Activator with Important AMPK-Independent Effects: A Systematic Review. *Cells*, **10**, 1095.
160. Musi, N., Hirshman, M.F., Nygren, J., Svanfeldt, M., Bavenholm, P., Rooyackers, O., Zhou, G., Williamson, J.M., Ljunqvist, O., Efendic, S., *et al.* (2002) Metformin increases AMP-activated protein kinase activity in skeletal muscle of subjects with type 2 diabetes. *Diabetes*, **51**, 2074–2082.
161. Young, L.H., Li, J., Baron, S.J. and Russell, R.R. (2005) AMP-Activated Protein Kinase: A Key Stress Signaling Pathway in the Heart. *Trends Cardiovasc. Med.*, **15**, 110–118.
162. Nikolaidis, S., Virgiliou, C., Vekiou, M., Skari, A., Kechagidou, A., Gika, H., Theodoridis, G., Pappas, P., Leondaritis, G. and Mougios, V. (2020) Effect of exercise on key pharmacokinetic parameters related to metformin absorption in healthy humans: A pilot study. *Scand. J. Med. Sci. Sports*, **30**, 858–864.

Appendix A

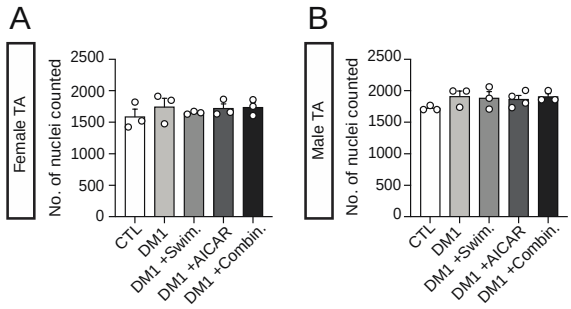

Figure A1. Total number of nuclei counted per TA cross-section for FISH analyses. (A) Female TA muscles, N = 3. (B) Male TA muscles, N = 3-4. One-way ANOVA was used followed by Tukey's post-hoc test.